A COMPRESSIVE MEASUREMENT MATRIX DESIGN FOR DETECTION AND TRACKING OF DIRECTION OF ARRIVAL USING SENSOR ARRAYS

A THESIS SUBMITTED TO

THE GRADUATE SCHOOL OF ENGINEERING AND SCIENCE

OF BILKENT UNIVERSITY

IN PARTIAL FULFILLMENT OF THE REQUIREMENTS FOR

THE DEGREE OF

MASTER OF SCIENCE

IN

ELECTRICAL AND ELECTRONICS ENGINEERING

By

Berk Özer

July 2016

A COMPRESSIVE MEASUREMENT MATRIX DESIGN FOR DETECTION AND TRACKING OF DIRECTION OF ARRIVAL USING SENSOR ARRAYS

By Berk Özer

July 2016

We certify that we have read this thesis and that in our opinion it is fully adequate, in scope and in quality, as a thesis for the degree of Master of Science.

Orhan Arıkan(Advisor)

Assoc. Prof. Dr. Sinan Gezici

Assoc. Prof. Dr. Ali Cafer Gürbüz

Approved for the Graduate School of Engineering and Science:

Levent Onural
Director of the Graduate School

ABSTRACT

A COMPRESSIVE MEASUREMENT MATRIX DESIGN FOR DETECTION AND TRACKING OF DIRECTION OF ARRIVAL USING SENSOR ARRAYS

Berk Özer
M.S. in Electrical and Electronics Engineering
Advisor: Orhan Arıkan
July 2016

Direction of Arrival (DoA) estimation is extensively studied in the array signal processing with many applications areas including radar, sonar, medical diagnosis and radio astronomy. Since, in sparse target environments, Compressive Sensing (CS) provides comparable performance with the classical DoA estimation techniques by using fewer number of sensor outputs, there are a multitude of proposed techniques in the literature that focus on surveillance (detection) and tracking (estimation) of DoA in CS framework. Many of such works elaborate on recovery of compressed signal and employ random measurement matrices, such as Bernoulli or Gaussian matrices. Although random matrices satisfy Restricted Isometry Property (RIP) for reconstruction, the measurement matrices can be designed to provide improved performance in search sectors that they are designed for.

In this thesis, a novel technique to design compressive measurement matrices is proposed in order to achieve enhanced DoA surveillance and tracking performance using sensor arrays. Measurement matrices are designed in order to minimize the Crameŕ-Rao Lower Bound (CRLB), which provides a lower bound for DoA estimation error. It is analytically shown that the proposed design technique attains the CRLB under mild conditions. Built upon the characteristics of proposed measurement design approach, a sequential surveillance technique using interference cancellation is introduced. A novel partitioning technique, which provides a greedy type solution to a minmax optimization problem, is also developed to ensure robust surveillance performance. In addition, an adaptive target tracking algorithm, which adaptively updates measurement matrices based on the available information of targets, is proposed. Via a comprehensive set of simulations,

it is demonstrated that the proposed measurement design technique facilities significantly enhanced surveillance and tracking performance over the widely used random matrices in the compressive sensing literature.

Keywords: DoA Estimation, Compressive Sensing, Array Signal Processing, Tracking, Surveillance.

ÖZET

ALGILAYICI DIZILIMI KULLANILARAK VARIŞ AÇISI SEZİMİ VE TAKİBİ İÇİN SIKIŞTIRMA MATRİSİ DİZAYNI

Berk Özer
Elektrik ve Elektronik Mühendisliği, Yüksek Lisans
Tez Danışmanı: Orhan Arıkan
Temmuz 2016

Varış açısı (VA) kestirimi, radar, sonar, tıbbi teşhis veya radyo astronomisi gibi birçok dizi sinyal işleme uygulamasında sıklıkla çalışılmış bir konudur. Sıkıştırmalı algılama (SA) yöntemleri, seyrek sahneler için klasik VA teknikleri ile kıyaslandığında benzer bir performansı daha az sayıda algılayıcı çıktısı kullanarak gösterebildiğinden, literatürde VA sezim (gözetleme) ve kestirimini (takibini) SA kullanarak yapan birçok çalışma yer almaktadır. Bu çalışmaların büyük bir bölümü daha çok geri çatım kısmına odaklanmakta ve ölçüm matrisi olarak Gaussian ve Bernoulli gibi rastgele matrisleri kullanmaktadır. Rastgele matrisler geri çatım için gerekli olan kısıtlanmış izometri özelliğini sağlasa da, gözetleme ve takip performansı ölçüm matrislerinin uygun bir şekilde seçilmesiyle artırılabilir.

Bu tezde, geliştirilen yeni bir teknik ile ölçüm matrisleri VA gözetleme ve takip performansını artıracak sağlayacak şekilde tasarlanmıştır. Ölçüm matrisleri VA kestiriminde yapılan hataya bir alt sınır veren Cramer-Rao -Rao Alt Sınırını (CRAS) en azaltacak şekilde dizayn edilmiştir. Sağlaması zor olmayan çeşitli şartlar altında, önerilen tekniğin CRAS'a ulaştığı analitik olarak gösterilmiştir. Önerilen ölçüm matrisi dizayn tekniğini ile girişim giderimi kullanarak ardışık gözetleme yapan yeni bir teknik önerilmiştir. Minmax tipindeki bir eniyileme problemine Greedy tipinde bir çözüm sağlayan yeni geliştirilen bir teknik ile, parametre uzayı gürbüz bir gözetleme performansı sağlayacak şekilde parçalara ayrılmıştır. Ayrıca, ölçüm matrislerini hedeflerinin bir sonraki pozisyonlarını tahmin ederek güncelleyen, uyarlamalı bir hedef takip algoritması geliştirilmiştir. Yapılan birçok simülasyon ile, önerilen ölçüm matrisi dizayn tekniğinin literatürde sıklıkla kullanılan Gaussian matrislere göre çok daha iyi bir gözetleme ve takip performansı sunduğu gösterilmiştir.

Anahtar sözcükler: Varış Açısı Kestirimi, Sıkıştırmalı Algılama, Sensör Dizilim Sinyal İşleme, Takip, Gözetleme.

Acknowledgement

I would like to thank my supervisor Prof. Dr. Orhan Arıkan for his support, guidance, suggestions throughout my studies with him starting from my junior year at the Bilkent University.

I want to articulate my gratitude to Assoc. Prof. Dr. Ali Cafer Gürbüz for his comments and suggestions to articles I authored throughout my studies. I also would like to express my special thanks to Assoc. Prof. Dr. Sinan Gezici for his contributions to interpret various cases and develop techniques in this thesis.

I thank Anastasia Lavrenko, Dr. Florian Romer and Prof. Dr. Giovanni Del Galdo of Fraunhofer IIS for their suggestions to expand the discussion in this thesis.

I also appreciate the financial and technical support from TUBITAK within 1001 research program grant with project number 113E515.

I am also grateful to Prof. Dr. Orhan Arıkan, Assoc. Prof. Dr. Sinan Gezici and Assoc. Prof. Dr. Ali Cafer Gürbüz for reading this thesis and being a member of my thesis committee.

Finally, but most significantly, I would articulate my gratitude to my parents, Figen and Metin Özer, for their love, sacrifices and invaluable support.

Contents

List of Figures

List of Tables

Chapter 1

Introduction

In this section, the primary problem investigated in this thesis, Direction of Arrival (DoA) surveillance and tracking, is first briefly introduced in 1.1. Another major concept of this thesis, Compressing Sensing (CS) theory, is summarized in Section 1.2. Some of the significant techniques that propose DoA estimation within CS framework are introduced in Section 1.3. Afterwards, the proposed methods in the literature that aim to design measurement matrices depending various criteria are discussed in Section 1.4 while the techniques related with the CRLB minimization are emphasized. Then, the main contributions of this thesis are briefly stated and the organization of the thesis is depicted in Section 1.5. Section 1.6 is dedicated to nomenclature tabulating the important notations and their descriptions.

1.1 Direction of Arrival (DoA) Estimation

Array signal processing techniques are designed to detect the presence of targets that emit electromagnetic and acoustic waves, that impinge on a sensor array. In the surveillance phase, the aim is to detect the presence of targets. Once a target is detected, its Direction of Arrival (DoA) relative to reference sensor is

estimated. DoA estimation has many applications such as radar [1, 2, 3], sonar [4, 5, 6], medical diagnosis [7, 8, 9] and wireless communications [10, 11, 12]. Thus, beginning from the early 1930s [13], many works in the literature focused on estimation of DoA. Among many techniques [2, 14, 15, 16, 17] in the literature, techniques providing spectrum estimations based on decomposition of eigenvalues, such as Multiple Signal Classification (MUSIC) [18] and Estimation Signal Parameters via Rotational Invariance Technique (ESPRIT) [19], are considered the most popular.

1.2 Compressive Sensing

The compressive sensing (CS) theory states that a signal which admits sparse representation in a certain basis can be reconstructed from a fewer number of samples than that required by Nyquist theorem [20, 21]. Let $\boldsymbol{x}$ be a K-sparse signal in $\mathbb{C}^{N\times N}$ sparsifying basis $\boldsymbol{\Psi}$ and $\boldsymbol{\mathcal{W}}$ be a measurement matrix. Then, it is possible to recover $\boldsymbol{x}$ from measurements $\boldsymbol{y} = \boldsymbol{\mathcal{W}x}$ as a solution of the following convex ℓ_1-optimization problem

$$\min ||\boldsymbol{s}||_1 \text{ s.t. } \boldsymbol{y} = \boldsymbol{\Theta s}, \tag{1.1}$$

where $\boldsymbol{\Theta} = \boldsymbol{\mathcal{W}\Psi}$ is the sensing matrix satisfying restricted isometry property (RIP) [20, 21, 22, 23]. According to the RIP, $\boldsymbol{x}$ can be recovered exactly using only $M = cK\log(N/K) \ll N$ measurements, where c is a small constant. Therefore, the CS framework can be utilized in many applications where comparable performance with classical techniques is attained using a much fewer number of measurements, reducing both complexity and hardware cost.

1.3 Compressive Sensing Techniques for Direction of Arrival Estimation

CS techniques are successfully applied to direction-of-arrival (DoA) estimation problems [24, 25, 26, 27, 28, 29, 30, 31], which are extensively studied in the areas of array signal processing, sensor networks, remote sensing, etc. Common approaches in DoA estimation, such as multiple signal classification (MUSIC) or generalized cross correlation (GCC) [32], require N measurements corresponding to Nyquist-rate sampling, where N is defined above. Typically, CS techniques are exploited for DoA problems by taking only M measurements via $\boldsymbol{\mathcal{W}}$ and estimating the DoA by means of sparse-reconstruction algorithms, such as matching pursuit [33], orthogonal matching pursuit (OMP) [34] and iterative hard/soft thresholding (IHT) [35]. Such techniques generally require a known grid $\widehat{\boldsymbol{\Psi}}$, where $\boldsymbol{x}$ is assumed to be sparse on the space spanned by $\widehat{\boldsymbol{\Psi}}$. In this case, DoA can be estimated by the estimation of the support of $\boldsymbol{x}$, i.e., the localization of non-zero positions on $\widehat{\boldsymbol{\Psi}}$.

Many works in the literature apply sparse reconstruction for the DoA estimation problem assuming an exactly known $\boldsymbol{\Psi}$ [25, 26]. The studies in [27, 28, 29] address the issue when $\boldsymbol{\Psi}$ is partially known, where the unknown part $\boldsymbol{\delta\Psi}$ is caused by various reasons such as basis mismatches, off-grid targets and modeling errors. Such problems are usually tackled by basis learning algorithms or in the context of off-grid reconstruction techniques [27, 36, 17, 37]. On the other hand, there is not much work in the literature on the design of $\boldsymbol{\mathcal{W}}$. This situation stems from the fact that a random $\boldsymbol{\mathcal{W}}$(e.g., with entries can be chosen from a Gaussian or symmetric Bernoulli distribution) is sufficiently incoherent with an orthogonal $\boldsymbol{\Psi}$ with high probability [22, 23], where the (mutual) coherence between $\boldsymbol{\mathcal{W}}$ and $\boldsymbol{\Psi}$ refers to another form of the RIP condition. Hence, in the majority of studies, $\boldsymbol{\mathcal{W}}$ is designated as a random Gaussian matrix whose entries are chosen as independent and identically distributed (i.i.d.) Gaussian.

1.4 Measurement Matrix Design for Direction of Arrival Surveillance and Tracking

Although Gaussian matrices satisfy the RIP condition with overwhelming probability, they do not necessarily yield the best performance in terms of the minimal coherence with $\boldsymbol{\Psi}$. In [38, 39], to assign $\boldsymbol{\mathcal{W}}$, an iterative approach is employed to minimize the sum of all cross-columns in $\boldsymbol{\Theta}$ for given $\boldsymbol{\Psi}$. In [40], $\boldsymbol{\mathcal{W}}$ and $\boldsymbol{\Psi}$ are simultaneously designed by forcing the Gram sense matrix $\boldsymbol{\Theta}^T\boldsymbol{\Theta}$ as close to the identity matrix as possible. In [41, 42] and [43], $\boldsymbol{\mathcal{W}}$ is designated to minimize some form of coherence with $\boldsymbol{\Psi}$ which is specifically formulated for multiple-input multiple-output (MIMO) and cognitive radar. Basically, all of such methods aim to design $\boldsymbol{\mathcal{W}}$ so that different versions of coherence between $\boldsymbol{\mathcal{W}}$ and $\boldsymbol{\Psi}$ are minimized. The main motivation behind this approach is embedded in the RIP condition, where the minimization of mutual coherence leads to exact reconstruction by a fewer number of measurements. Therefore, using mutual coherence as a design criterion for $\boldsymbol{\mathcal{W}}$ aims to minimize M while exact reconstruction is still guaranteed.

In the literature, the design of $\boldsymbol{\mathcal{W}}$ is also performed using task-driven criteria rather than coherence. In these techniques, the general idea is to optimize an objective function corresponding to a specific task, where the number of measurements is usually regarded as a fixed parameter. In [44], $\boldsymbol{\mathcal{W}}$ is selected so that the mutual information between past measurements and the unknown class or the underlying signal is maximized for the purpose of detection and reconstruction, respectively. In [45], an optimization framework is proposed for various task-specific goals, such as regression and multi-class classification. In [46], maximization of Fisher Information (FI) is utilized as a design criterion for $\boldsymbol{\mathcal{W}}$ in order to improve detection performance of beamformers. In [47], $\boldsymbol{\mathcal{W}}$ is optimized to maximize the array gain $\boldsymbol{\mathcal{W}}(\boldsymbol{\theta}_1)\boldsymbol{\Psi}(\boldsymbol{\theta}_1)$ for DoA $\boldsymbol{\theta}_1$ while cross correlation $\boldsymbol{\mathcal{W}}(\boldsymbol{\theta}_1)\boldsymbol{\Psi}(\boldsymbol{\theta}_2)$, $\forall \boldsymbol{\theta}_1 \neq \boldsymbol{\theta}_2$ is minimized. In [48], $\boldsymbol{\mathcal{W}}$ is designed by minimizing of Crameŕ-Rao Lower Bound (CRLB) while false detection probability is below a threshold. Since it is very challanging to obtain $\boldsymbol{\mathcal{W}}$ in closed form, numerical

optimization techniques (local minimizer) are applied. In [49] and [50], $\boldsymbol{\mathcal{W}}$ is designed so as to minimize the (CRLB) for the parameter of interest for a single target.

1.5 Contribution and Organization

The main contributions of this thesis can be summarized as follows:

- A novel measurement matrix design technique is proposed based on the minimization of the CRLB to enhance both surveillance and tracking of targets using sensor arrays. The proposed method jointly minimizes the CRLB for two parameters of interest of a target, elevation and azimuth angle.
- It is proved that the proposed measurement matrices achieve the CRLB (Theorem 1) under mild conditions.
- A new sequential Bayesian detection approach is proposed for surveillance (Algorithm 1).
- The surveillance space is partitioned by a proposed partitioning technique, which is used by the proposed sequential Bayesian detection approach (Algorithm 2).
- An adaptive target tracking algorithm is developed (Algorithm 3).
- An algorithm to jointly perform surveillance and tracking for multiple targets is proposed (Algorithm 4).
- Via a set of simulations, it is illustrated that the proposed measurement matrices and the corresponding detection and tracking techniques significantly outperform the widely used random matrices in the compressive sensing literature.

The remaining of this thesis is organized as follows. In Chapter 2 firstly the signal model and the corresponding definitions are given in Section 2.1. Then, in Section 2.2, the cost function to minimize the CLRB for parameter of interest is derived. A measurement matrix design technique is introduced and it is analytically proved that the proposed measurement matrices provide the optimal solution with the minimum CRLB by Proposition 1 and Theorem 1.

The detection (surveillance) and tracking techniques built upon the proposed measurement matrices are developed for the case of a single target in Chapter 3. In Section 3.1.1, a novel algorithm, called sequential surveillance with interference cancellation (*SSIC*), is introduced. In Section 3.1.2, first a minmax type optimization is formed to partition the paramter space in order to ensure robust surveillance performance. Afterwards, a novel Greedy type algorithm is proposed to solve the minimax optimization problem. Finally, in Section 3.2, an adaptive tracking algorithm, which updates proposed measurement matrices using the predicted DoA of upcoming snapshots, is introduced.

In Chapter 4, the proposed techniques for the detection and tracking of a single target in Chapter 3 are extended to multiple targets in scene. An algorithm, as referred to as Adaptive Tracking of Multiple Targets using Successive Interference Cancellation (*ATSIC*), is developed in order to successively cancel the interference while adaptively updating the measurement matrices with the proposed technique in Section 2.2. Futhermore, in Section 4.2, a novel technique built upon proposed *ATSIC* and *SSIC* (Section 3.1.1) is introduced so as to jointly perform surveillance and tracking of multiple targets in the scene.

In Chapter 5, the detection and tracking performance of the proposed techniques are evaluated and compared via a comprehensive set of simulations. In Section 5.1, the estimation techniques and the error functions are first defined. Then, the CRLB obtained by the proposed and Gaussian measurement matrices are compared. The estimation error is also illustrated and compared the corresponding CRLB. In addition, the CRLB and the estimation error with the proposed and Gaussian measurement matrices are demonstrated as a function of

Table 1.1: Notations and their description used in the thesis

Notation	**Description**
γ_k	Elevation angle of k^{th} target
ϕ_k	Azimuth angle of k^{th} target
$\boldsymbol{\theta}_k$	Elevation and azimuth of k^{th} target
$x_n(t)$	The signal received at n^{th} sensor
$y_m(t)$	Analog compressed measurements.
$\boldsymbol{y}$	Measurement vector.
$\boldsymbol{W}$	Measurement matrix.
$\boldsymbol{\mathcal{W}}$	Extended measurement matrix.
$\text{Tr}\{\boldsymbol{J}^{-1}(\boldsymbol{W},\boldsymbol{\theta})\}$	The CRLB evulated at $\boldsymbol{\theta}$ using $\boldsymbol{W}$.
$\boldsymbol{W}_{\boldsymbol{\theta}}$	The measurement matrix designed on $\boldsymbol{\theta}$.
$\boldsymbol{W}_R$	Random (Gaussian) measurement matrix.
$\boldsymbol{J}(\boldsymbol{W},\boldsymbol{\theta})$	Fisher Information matrix evaluated at $\boldsymbol{\theta}$ by using $\boldsymbol{W}$.
$\mathcal{S}_b$	b^{th} sector of the parameter space.
$\widetilde{\boldsymbol{\theta}}_b$	The design vector of b^{th} sector.
$\boldsymbol{\theta}_0$	The DoA of a single target of interest.
$\boldsymbol{\theta}_D$	The (known) design vector.

Signal-to-Noise (SNR). In Section 5.2.1 and Section 5.2.2, the sensitivity (performance degradation) of the proposed measurement design technique is evaluated under the case of perturbed design point, i.e., the design angle is perturbed from actual DoA. In Section 5.2.3, the sensitivity of the proposed technique is assessed under the case of unknown complex amplitude and perturbed design point. The remaining of Chapter 5 elaborates on the performance of the proposed detection and tracking techniques. In Section 5.3.1, the parameter space is partitoned by the technique introduced in 3.1.2. The sectors and their corresponding optimalities are illustrated. The performance is measured by the number of sectors. In Section 5.3.2, the Receiver Operating Characteristics (ROC) analysis of *SSIC* is performed. The performance of proposed adaptive tracking technique is discussed in Section 5.4. Finally, the performance of *ATSIC* is illustrated in Section 5.5.

Chapter 6 is allocated to draw conclusions. In Appendix A and Appendix B, the CRLB is derived under the case of known and unknown complex amplitude, respectively. In Appendix C, it is proved that derivative of steering vectors are orthogonal for symmetric array configurations.

1.6 Nomenclature

Table 1.1 covers the important notations and the corresponding descriptions throughout this thesis.

Chapter 2

The Signal Model and Measurement Matrix Design

In this chapter, the signal model that provides compressed sensor outputs is first introduced in Section 2.1. Following the description of array geometry, received signal of individual array elements are formulated. Unlike commonly used approaches, that compress the sensor outputs after Analog-to-Digital Converter (ADC), the array outputs are compressed by using an analog combiner before ADC. In the design of combiner, an optimization approach that aims to minimize the CRLB is followed. In Section 2.2.1 and in Section 2.2.2, the cost function to minimize the CRLB over compressive measurement matrices is defined and a measurement matrix design technique that minimizes the CRLB is introduced, respectively. It is analytically proved that the proposed technique minimizes the CRLB by using measurement matrices consisting of 2 orthonormal rows in total, that are allocated for elevation and azimuth.

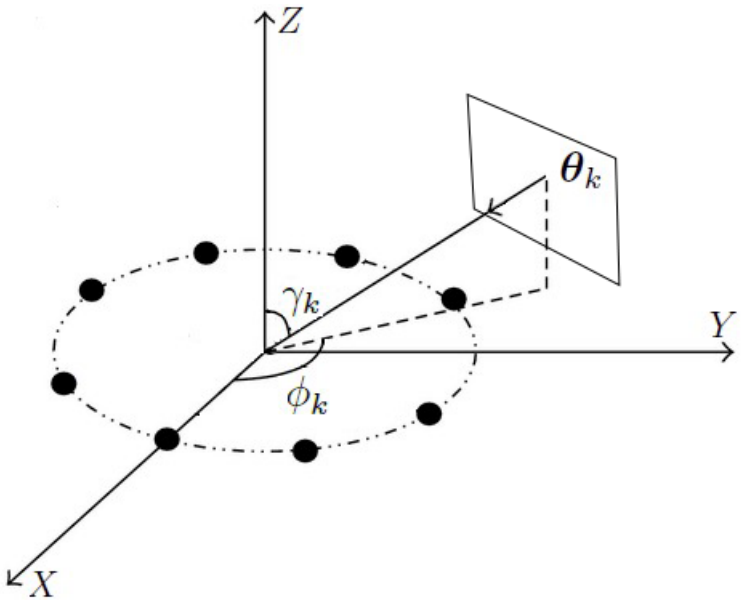

Figure 2.1: Elevation γ_k and azimuth ϕ_k angle of the impinging signal from far-field source k.

2.1 Signal Model

As demonstrated in Fig. 2.1, $\boldsymbol{\theta}_k = [\gamma_k \ \phi_k]$ denotes the angular orientation of a plane wave impinging from the k^{th} target on some N-element array, where $\gamma_k \in \left[0, \ \frac{\pi}{2}\right]$ and $\phi_k \in [0, \ \pi]$ represent the elevation and azimuth angles, respectively. In the presence of K targets in the far field of the array, the (baseband) signal received at the n^{th} sensor is given by

$$x_n(t) = \sum_{k=1}^{K} s_k e^{j\omega(t+\tau_n(\boldsymbol{\theta}_k))}, \tag{2.1}$$

where ω is the carrier frequency, and $\tau_n(\boldsymbol{\theta}_k)$ and s_k are the relative time delay and the complex amplitude of the signal impinging from direction $\boldsymbol{\theta}_k$, respectively.

The relative time delay of the k^{th} target at the n^{th} sensor is calculated as

$$\tau_n(\boldsymbol{\theta}_k) = \frac{\boldsymbol{P}_n^T}{c}\boldsymbol{\zeta}(\boldsymbol{\theta}_k) \tag{2.2}$$

where $\boldsymbol{P}_n^{\text{T}}$ is the vector of relative positions of the n^{th} sensor with respect to the reference point, c denotes the speed of wave and $\boldsymbol{\zeta}(\boldsymbol{\theta}_k)$ is the direction array

defined as:

$$\boldsymbol{\zeta}\left(\boldsymbol{\theta}_k\right) = \begin{bmatrix} \sin\left(\gamma_k\right)\cos\left(\phi_k\right) \\ \sin\left(\gamma_k\right)\sin\left(\phi_k\right) \\ \cos\left(\gamma_k\right) \end{bmatrix}. \tag{2.3}$$

To reduce the number of channels to be sampled from N to M ($M < N$), unlike the classical CS techniques, an analog pre-combiner at the sensor outputs is employed as depicted in Fig. 2.2. This allows us to decrease the number of ADCs and the amount of data to be processed while preserving a larger aperture. Denoting by $y_m(t)$ the signal at the m^{th} output of such a combiner, the signal at the m^{th} combiner output is given by

$$\begin{aligned} y_m(t) &= \sum_{n=1}^{N} w_{mn}\left(x_n\left(t\right) + n(t)\right) \\ &= \sum_{n=1}^{N}\sum_{k=1}^{K} w_{mn}(s_k e^{j\omega(t+\tau_n(\boldsymbol{\theta}_k))} + n(t)), \end{aligned} \tag{2.4}$$

where w_{mn} is the weight of the n^{th} sensor in the m^{th} combiner channel and $n(t)$ is circularly symmetric Gaussian noise with variance σ_n^2. Then, combining M channel outputs, analog measurement vector $\boldsymbol{y}(t)$ in $\mathbb{C}^{M\times 1}$ can be written as

$$\boldsymbol{y}(t) = \boldsymbol{W}\left(\sum_{k=1}^{K}\boldsymbol{x}\left(\boldsymbol{\theta}_k, s_k, t\right) + \boldsymbol{n}(t)\right), \tag{2.5}$$

where $\boldsymbol{W} = \left\{\left\{w_{mn}\right\}_{n=1}^{N}\right\}_{m=1}^{M}$ in $\mathbb{C}^{M\times N}$ is the measurement matrix and $\boldsymbol{x}\left(\boldsymbol{\theta}_k, s_k, t\right) = \left\{s_k e^{j\omega(t+\tau_n(\boldsymbol{\theta}_k))}\right\}_{n=1}^{N}$ in $\mathbb{C}^{N\times 1}$ represents the outputs of N sensors at time t.

Using the set of N_T time instances $\boldsymbol{t} = [t_1\ t_2\ ...\ t_{N_T}]$, the set of measurement vectors at N_T time samples can be combined into an $MN_T \times 1$ observation vector $\boldsymbol{y}$ as follows

$$\boldsymbol{y} = \boldsymbol{\mathcal{W}}\left(\sum_{k=1}^{K}\boldsymbol{x}\left(\boldsymbol{\theta}_k, s_k, \boldsymbol{t}\right) + \boldsymbol{n}\right), \tag{2.6}$$

where $\boldsymbol{n} \sim \mathcal{CN}\left(\boldsymbol{0}, \sigma_n^2\boldsymbol{I}_{MN_T}\right)$ and $\boldsymbol{\mathcal{W}} = \boldsymbol{W}\otimes\boldsymbol{I}_{N_T}$ and $\boldsymbol{x}\left(\boldsymbol{\theta}_k, s_k, \boldsymbol{t}\right) = \boldsymbol{x}\left(\boldsymbol{\theta}_k, s_k, 0\right)\otimes e^{j\omega\boldsymbol{t}}$ with $\boldsymbol{I}_u$ being the $u \times u$ identity matrix and $\otimes$ denoting the Kronecker product.

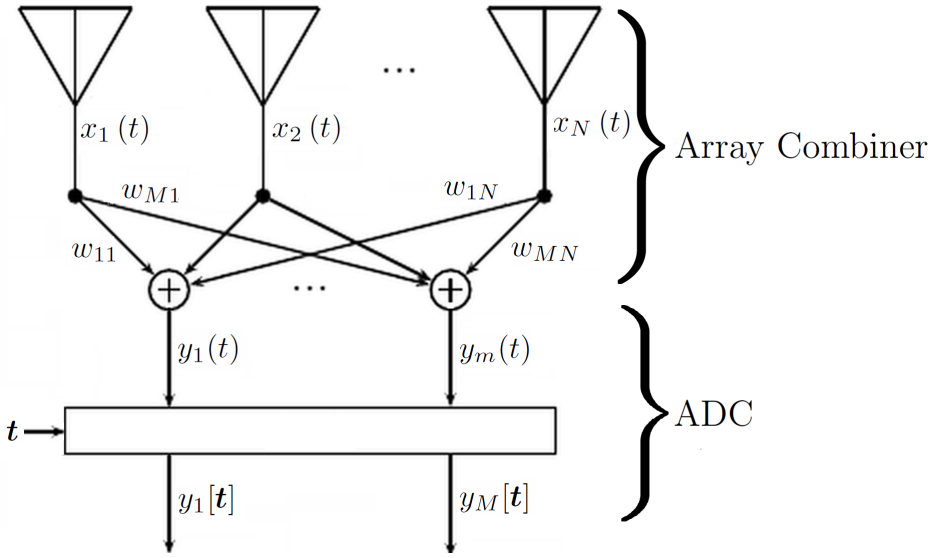

Figure 2.2: Compressive sensor array with analog array combiner and Analog-to-Digital Converter (ADC).

2.2 Measurement Matrix Design Based on the CRLB Minimization

In this section, a measurement design technique, which forms the basis for the proposed surveillance and tracking algorithms in Chapter 3 and Chapter 4 is proposed. To improve both surveillance and tracking performance, as elaborated on in Section 3.1 and Section 3.2, measurement matrices are designed such that the DoA parameter can be estimated with low errors .For this reason, the minimization of the CRLB related to the DoA parameters of the targets is considered instead of assuming a prior knowledge on DoA distribution as in the case of Bayesian CRLB. Since the analytical minimization of the CRLB for multiple targets is an open problem, the CRLB for a single target is analytically minimized in Chapter 2 and extensions for multiple targets are presented in Section 4.1. For symmetric sensor arrays, it is proved that the proposed technique attains the optimum performance in terms of the CRLB minimization.

When a single target is present the scene, the measurements captured by measurement matrix $\boldsymbol{W}$ can be written by expanding (2.6) as follows

$$\begin{aligned}\boldsymbol{y} &= \boldsymbol{\mathcal{W}}\left(\boldsymbol{x}\left(\boldsymbol{\theta}, s, \boldsymbol{t}\right) + \boldsymbol{n}\right) \\ &= \left(\boldsymbol{W} \otimes \boldsymbol{I}_{N_T}\right)\left(s e^{j\frac{\omega}{c}\boldsymbol{P}_n^T \boldsymbol{\zeta}(\boldsymbol{\theta})} \otimes e^{j\omega \boldsymbol{t}} + \boldsymbol{n}\right),\end{aligned} \tag{2.7}$$

where $\boldsymbol{W}$, $\boldsymbol{P}_n$ and $\boldsymbol{t}$ are controlled parameters, ω is assumed to be known and $\boldsymbol{\theta}$ is the parameter of interest.

If the complex amplitude s is kept as deterministic but unknown, it can be considered as a nuisance parameter and the 3×3 inverse Fisher Information matrix becomes the following

$$\boldsymbol{J}_{\boldsymbol{\theta}}^{-1}\left(\boldsymbol{W}, \boldsymbol{\theta}, s\right) = \begin{bmatrix} J_{\gamma}\left(\boldsymbol{W}, \boldsymbol{\theta}, s\right) & J_{\gamma\phi}\left(\boldsymbol{W}, \boldsymbol{\theta}, s\right) \\ J_{\gamma\phi}\left(\boldsymbol{W}, \boldsymbol{\theta}, s\right) & J_{\phi}\left(\boldsymbol{W}, \boldsymbol{\theta}, s\right) \end{bmatrix}^{-1}, \tag{2.8}$$

as detailed derivations of $J_{\gamma}\left(\boldsymbol{W}, \boldsymbol{\theta}, s\right)$, $J_{\gamma\phi}\left(\boldsymbol{W}, \boldsymbol{\theta}, s\right)$ and $J_{\phi}\left(\boldsymbol{W}, \boldsymbol{\theta}, s\right)$ are given in Appendix B.

Since the analytical minimization of $\mathrm{Tr}\left\{\boldsymbol{J}_{\boldsymbol{\theta}}^{-1}\left(\boldsymbol{W}, \boldsymbol{\theta}, s\right)\right\}$ over $\boldsymbol{W}$ is an open problem including challenging cases, e.g., even in the main diagonal elements alone, the Gram matrix of $\boldsymbol{W}$ appears at least three times, a practical approach is followed. Assuming that s is known prior to the CRLB computation, the minimization of $\mathrm{Tr}\left\{\boldsymbol{J}_{\boldsymbol{\theta}}^{-1}\left(\boldsymbol{W}, \boldsymbol{\theta}, s\right)\right\}$ over $\boldsymbol{W}$ becomes analytically tractable and independent of s as shown in the next sections. Thus, a proper optimization problem to minimize the CRLB for $\boldsymbol{\theta}$ over $\boldsymbol{W}$ is formed in Section 2.2.1 and the corresponding closed form solution is given in Section 2.2.2 by assuming s is known prior the design of measurement matrices. In addition, as the performance of the proposed technique is evaluated in the case unknown complex amplitude in Section 5.2.3, the performance of proposed technique gracefully degrades for feasible SNR levels.

2.2.1 The Cost Function of the Optimization Framework

The aim is to perform the optimal design of measurement matrix $\boldsymbol{W}$ to minimize the CRLB for estimating $\boldsymbol{\theta}$. Since maximum likelihood estimators can attain the CRLB under certain circumstances, minimization of the CRLB corresponds to the minimization of the estimation error for $\boldsymbol{\theta}$ [51, 52]. Furthermore, the CRLB minimization provides an optimization framework which is independent of the estimator. Thus, the cost function is defined as

$$\begin{aligned} \boldsymbol{W}_{\boldsymbol{\theta}} = \arg\min_{\boldsymbol{W}} \quad & \mathrm{Tr}\left\{\boldsymbol{J}^{-1}\left(\boldsymbol{W},\boldsymbol{\theta}\right)\right\} \\ \text{s.t.} \quad & \boldsymbol{W}\boldsymbol{W}^{\mathrm{H}} = \boldsymbol{I}_M, \end{aligned} \tag{2.9}$$

where $\boldsymbol{I}_M$ denotes an $M \times M$ identity matrix and $\mathrm{Tr}\left\{\boldsymbol{J}^{-1}\left(\boldsymbol{W},\boldsymbol{\theta}\right)\right\}$ refers to the trace of the inverse Fisher Information matrix evaluated at $\boldsymbol{\theta}$. The constraint $\boldsymbol{W}\boldsymbol{W}^{\mathrm{H}} = \boldsymbol{I}_M$ in (2.9) ensures that $\boldsymbol{W}$ is full rank, i.e., it provides non-redundant set of measurements, and avoids coloring the noise[1] $\mathrm{Tr}\left\{\boldsymbol{J}^{-1}\left(\boldsymbol{W},\boldsymbol{\theta}\right)\right\}$ refers to the trace of the inverse Fisher Information matrix evaluated at $\boldsymbol{\theta}$ and is given by

$$\mathrm{Tr}\left\{\boldsymbol{J}^{-1}\left(\boldsymbol{W},\boldsymbol{\theta}\right)\right\} = \frac{J_\gamma\left(\boldsymbol{W},\boldsymbol{\theta}\right) + J_\phi\left(\boldsymbol{W},\boldsymbol{\theta}\right)}{J_\gamma\left(\boldsymbol{W},\boldsymbol{\theta}\right) J_\phi\left(\boldsymbol{W},\boldsymbol{\theta}\right) - \left(J_{\gamma\phi}\left(\boldsymbol{W},\boldsymbol{\theta}\right)\right)^2}, \tag{2.10}$$

where

$$J_\gamma\left(\boldsymbol{W},\boldsymbol{\theta}\right) = \frac{1}{c_0}\left(\boldsymbol{d}_\gamma\left(\boldsymbol{\theta}\right)\right)^H \boldsymbol{W}^H\boldsymbol{W}\boldsymbol{d}_\gamma\left(\boldsymbol{\theta}\right), \tag{2.11}$$

$$J_\phi\left(\boldsymbol{W},\boldsymbol{\theta}\right) = \frac{1}{c_0}\left(\boldsymbol{d}_\phi\left(\boldsymbol{\theta}\right)\right)^H \boldsymbol{W}^H\boldsymbol{W}\boldsymbol{d}_\phi\left(\boldsymbol{\theta}\right), \tag{2.12}$$

$$J_{\gamma\phi}\left(\boldsymbol{W},\boldsymbol{\theta}\right) = \frac{1}{c_0}\left(\boldsymbol{d}_\gamma\left(\boldsymbol{\theta}\right)\right)^H \boldsymbol{W}^H\boldsymbol{W}\boldsymbol{d}_\phi\left(\boldsymbol{\theta}\right), \tag{2.13}$$

and

$$c_0 = \frac{\sigma_n^2}{N_T|s|^2}, \tag{2.14}$$

$$\boldsymbol{d}_\gamma\left(\boldsymbol{\theta}\right) = \frac{\omega}{c}\left(\boldsymbol{P}_n^T\frac{\partial\boldsymbol{\zeta}\left(\boldsymbol{\theta}\right)}{\partial\gamma}\right) \otimes e^{j\omega\boldsymbol{\zeta}(\boldsymbol{\theta})}, \tag{2.15}$$

$$\boldsymbol{d}_\phi\left(\boldsymbol{\theta}\right) = \frac{\omega}{c}\left(\boldsymbol{P}_n^T\frac{\partial\boldsymbol{\zeta}\left(\boldsymbol{\theta}\right)}{\partial\phi}\right) \otimes e^{j\omega\boldsymbol{\zeta}(\boldsymbol{\theta})}, \tag{2.16}$$

as derived in Appendix A.

[1]Note that this constraint can be imposed on $\boldsymbol{W}$ without loss of generality since it can be shown that for every non-orthogonal $\boldsymbol{W}$ a corresponding orthogonal one that achieves the same CRLB can be found.

2.2.2 Optimal Measurement Design

Towards the aim of solving the optimization problem in (2.9), the following proposition presents a lower bound on the cost function in (2.9).

Proposition 1. *For a measurement matrix* $\boldsymbol{W}$ *that satisfies* $\boldsymbol{W}\boldsymbol{W}^H = \boldsymbol{I}_M$, $L(\boldsymbol{W}, \boldsymbol{\theta}) = c_0 \left(\frac{1}{\|\boldsymbol{d}_\gamma(\boldsymbol{\theta})\|^2} + \frac{1}{\|\boldsymbol{d}_\phi(\boldsymbol{\theta})\|^2} \right)$ *provides a lower bound for the CRLB as*

$$\mathrm{Tr}\left\{ \boldsymbol{J}^{-1}(\boldsymbol{W}_{\boldsymbol{\theta}}, \boldsymbol{\theta}) \right\} \geq L(\boldsymbol{W}, \boldsymbol{\theta}), \tag{2.17}$$

where c_0 *is as defined in (2.14).*

Proof. Let $\boldsymbol{W}^{\mathrm{H}} = [\widehat{\boldsymbol{w}}_1, \widehat{\boldsymbol{w}}_2, \cdots, \widehat{\boldsymbol{w}}_M]$ is an orthonormal set, i.e., $\|\widehat{\boldsymbol{w}}_m\|^2 = 1 \; \forall \, m$ and $\widehat{\boldsymbol{w}}_i^{\mathrm{H}} \widehat{\boldsymbol{w}}_j = 0 \; \forall \; i \neq j$. Then, the following relations can be obtained based on (2.10), (2.11) and (2.12).

$$\begin{aligned}
\mathrm{Tr}\left\{ \boldsymbol{J}^{-1}(\boldsymbol{W}, \boldsymbol{\theta}) \right\} &\geq \frac{J_\gamma(\boldsymbol{W}, \boldsymbol{\theta}) + J_\phi(\boldsymbol{W}, \boldsymbol{\theta})}{J_\gamma(\boldsymbol{W}, \boldsymbol{\theta}) \, J_\phi(\boldsymbol{W}, \boldsymbol{\theta})} \\
&= \frac{1}{J_\gamma(\boldsymbol{W}, \boldsymbol{\theta})} + \frac{1}{J_\phi(\boldsymbol{W}, \boldsymbol{\theta})} \\
&= \frac{c_0}{\sum_{m=1}^{M} \left| \boldsymbol{d}_\gamma(\boldsymbol{\theta})^{\mathrm{H}} \widehat{\boldsymbol{w}}_m \right|^2} + \frac{c_0}{\sum_{m=1}^{M} \left| \boldsymbol{d}_\phi(\boldsymbol{\theta})^{\mathrm{H}} \widehat{\boldsymbol{w}}_m \right|^2} \\
&\geq c_0 \left(\frac{1}{\|\boldsymbol{d}_\gamma(\boldsymbol{\theta})\|^2} + \frac{1}{\|\boldsymbol{d}_\phi(\boldsymbol{\theta})\|^2} \right),
\end{aligned}$$

where the first inequality is derived by removing the last term in the denominator in (2.10), the second equality is obtained from (2.11) and (2.12), and the last inequality follows from Cauchy-Schwarz inequality that:

$$\begin{aligned}
\left| \boldsymbol{d}_\gamma(\boldsymbol{\theta})^{\mathrm{H}} \widehat{\boldsymbol{w}}_m \right|^2 &\leq \left| \boldsymbol{d}_\gamma(\boldsymbol{\theta})^{\mathrm{H}} \boldsymbol{d}_\gamma(\boldsymbol{\theta}) \right|^2, \\
\left| \boldsymbol{d}_\phi(\boldsymbol{\theta})^{\mathrm{H}} \widehat{\boldsymbol{w}}_m \right|^2 &\leq \left| \boldsymbol{d}_\phi(\boldsymbol{\theta})^{\mathrm{H}} \boldsymbol{d}_\phi(\boldsymbol{\theta}) \right|^2,
\end{aligned}$$

for $\|\widehat{\boldsymbol{w}}_m\|^2 = 1 \forall \, m$ as proposed. □

Based on Proposition 1, the following theorem provides the solution of the optimal measurement matrix design problem in (2.9).

Theorem 1. *Let* $\widehat{\boldsymbol{d}_\gamma}(\boldsymbol{\theta}) = \frac{\boldsymbol{d}_\gamma(\boldsymbol{\theta})}{\|\boldsymbol{d}_\gamma(\boldsymbol{\theta})\|}$ *and* $\widehat{\boldsymbol{d}_\phi}(\boldsymbol{\theta}) = \frac{\boldsymbol{d}_\phi(\boldsymbol{\theta})}{\|\boldsymbol{d}_\phi(\boldsymbol{\theta})\|}$. *Then,* $\boldsymbol{W}_{\boldsymbol{\theta}} = \begin{bmatrix} \widehat{\boldsymbol{d}_\gamma}(\boldsymbol{\theta})^H \\ \widehat{\boldsymbol{d}_\phi}(\boldsymbol{\theta})^H \end{bmatrix}$ *is the optimal measurement matrix that minimizes the CRLB.*

Proof. To prove Theorem 1, it suffices to show that the measurement matrix $\boldsymbol{W}_{\boldsymbol{\theta}} = \begin{bmatrix} \widehat{\boldsymbol{d}_\gamma}(\boldsymbol{\theta})^{\mathrm{H}} \\ \widehat{\boldsymbol{d}_\phi}(\boldsymbol{\theta})^{\mathrm{H}} \end{bmatrix}$ allows to achieve $L(\boldsymbol{W}, \boldsymbol{\theta})$, which, according to Proposition 1, forms the lower bound for the CRLB. To that aim, (2.11) can be written as

$$\begin{aligned} J_\gamma(\boldsymbol{W}_{\boldsymbol{\theta}}, \boldsymbol{\theta}) &= \boldsymbol{d}_\gamma(\boldsymbol{\theta})^{\mathrm{H}} \begin{bmatrix} \widehat{\boldsymbol{d}_\gamma}(\boldsymbol{\theta}) & \widehat{\boldsymbol{d}_\phi}(\boldsymbol{\theta})^{\mathrm{H}} \end{bmatrix} \begin{bmatrix} \widehat{\boldsymbol{d}_\gamma}(\boldsymbol{\theta})^{\mathrm{H}} \\ \widehat{\boldsymbol{d}_\phi}(\boldsymbol{\theta})^{\mathrm{H}} \end{bmatrix} \boldsymbol{d}_\gamma(\boldsymbol{\theta}) \\ &= \boldsymbol{d}_\gamma(\boldsymbol{\theta})^{\mathrm{H}} \left(\widehat{\boldsymbol{d}_\gamma}(\boldsymbol{\theta}) \widehat{\boldsymbol{d}_\gamma}(\boldsymbol{\theta})^{\mathrm{H}} + \widehat{\boldsymbol{d}_\phi}(\boldsymbol{\theta}) \widehat{\boldsymbol{d}_\phi}(\boldsymbol{\theta})^{\mathrm{H}} \right) \boldsymbol{d}_\gamma(\boldsymbol{\theta}) \\ &= \frac{\left(\boldsymbol{d}_\gamma(\boldsymbol{\theta})^{\mathrm{H}} \boldsymbol{d}_\gamma(\boldsymbol{\theta})^{\mathrm{H}} \right)^2}{\boldsymbol{d}_\gamma(\boldsymbol{\theta})^{\mathrm{H}} \boldsymbol{d}_\gamma(\boldsymbol{\theta})^{\mathrm{H}}} = \|\boldsymbol{d}_\gamma(\boldsymbol{\theta})\|^2, \end{aligned} \tag{2.18}$$

where $\boldsymbol{d}_\phi(\boldsymbol{\theta})^{\mathrm{H}} \boldsymbol{d}_\gamma(\boldsymbol{\theta}) = 0$ (see Appendix C). Following the same procedure, it is easy to show that

$$J_\phi(\boldsymbol{W}_{\boldsymbol{\theta}}, \boldsymbol{\theta}) = \|\boldsymbol{d}_\phi(\boldsymbol{\theta})\|^2, \tag{2.19}$$

$$J_{\gamma\phi}(\boldsymbol{W}_{\boldsymbol{\theta}}, \boldsymbol{\theta}) = 0. \tag{2.20}$$

Substituting (2.18), (2.19) and (2.20) into (2.10), it is obtained that

$$\begin{aligned} \mathrm{Tr}\left\{ \boldsymbol{J}^{-1}(\boldsymbol{W}_{\boldsymbol{\theta}}, \boldsymbol{\theta}) \right\} &= c_0 \frac{\|\boldsymbol{d}_\gamma(\boldsymbol{\theta})\|^2 + \|\boldsymbol{d}_\phi(\boldsymbol{\theta})\|^2}{\|\boldsymbol{d}_\gamma(\boldsymbol{\theta})\|^2 \|\boldsymbol{d}_\phi(\boldsymbol{\theta})\|^2} \\ &= c_0 \left(\frac{1}{\|\boldsymbol{d}_\gamma(\boldsymbol{\theta})\|^2} + \frac{1}{\|\boldsymbol{d}_\phi(\boldsymbol{\theta})\|^2} \right). \end{aligned} \tag{2.21}$$

Therefore, the measurement matrix in the theorem achieves the lower bound on the CRLB specified in Proposition 1; hence, it becomes a solution of (2.9). □

Theorem 1 also illustrates that it is sufficient to use only the measurement matrix with 2 rows, i.e., $M = 2$, to reach the optimal performance in terms of the CRLB. Hence, $2N_T$ of measurements are used in $\boldsymbol{\mathcal{W}}_{\boldsymbol{\theta}} = \boldsymbol{W}_{\boldsymbol{\theta}} \otimes \boldsymbol{I}_{N_T}$.

Chapter 3

Surveillance and Tracking of a Single Target

In this Chapter, a novel surveillance and tracking technique built upon the proposed measurement matrices in the case of a single target in the scene. A novel algorithm, called sequential surveillance with interference cancellation (*SSIC*) is introduced in Section 3.1.1. A novel algorithm that forms a greedy type solution to a minmax type optimization problem ensuring robust surveillance performance is proposed in Section 3.1.2. Finally, in Section 3.2, an adaptive tracking algorithm, which updates proposed measurement matrices using the predicted DoA of upcoming snapshots, is developed.

3.1 Surveillance: Detection of a Newly Emerging Target by Using the Proposed Measurement Matrix Design

In this section, an enhanced surveillance of a newly emerging target in the scene is analyzed. A sequential surveillance approach and a corresponding partitioning

technique of the surveillance space are introduced in the proposed sequential enhanced surveillance approach.

3.1.1 Sequential Surveillance with Interference Cancellation (*SSIC*)

In the surveillance mode of operation, the aim is to detect possible newly emerging targets in the scene (surveillance space), i.e., $\mathcal{S} = [0,\ \frac{\pi}{2}] \times [0,\ \pi]$ (for γ and ϕ, respectively). To perform surveillance for $\mathcal{S}$, a sequential surveillance approach is adopted. Namely, $\mathcal{S}$ is partioned into a set of mutually exclusive collectively exhaustive (MECE) N_S sectors, represented by $\{\mathcal{S}_1, ..., \mathcal{S}_p, ..., \mathcal{S}_{N_S}\}$, and each sector is monitored at a single snapshot.

A properly designed measurement matrix is designated for each sector, i.e., newly arriving targets in sector $\mathcal{S}_p$ are detected by taking measurements via $\boldsymbol{W}_{\widetilde{\boldsymbol{\theta}}_p}$, where $\widetilde{\boldsymbol{\theta}}_p \in \mathcal{S}_p$. In such a sequential approach, the surveillance is conducted for the entire surveillance space within N_S snapshots. Since $2N_T$ measurements are utilized for each sector, as described Section 2.2, $2N_T N_S$ measurements are collected in order to span the entire surveillance space.

The details of the proposed approach are illustrated in Algorithm 1, which is referred to as *SSIC*. In the *SSIC* algorithm, measurements are sequentially captured by a properly designed measurement matrix and the interference from currently tracked targets are cancelled as described in detail in Section 4.2. Then, the parameter of interest $\boldsymbol{\theta}$ and the unknown nuisance parameter s are estimated by employing gradient descent techniques for estimation. Note that such gradient descent techniques can be generalized to any type of DOA estimator in the compressed domain [17, 37, 53, 54, 55, 56].

The primary motivation for the sequential Bayesian detection is that the proposed measurement design technique yields the best estimation performance (in terms of the CRLB) when an emerging target coincides with the design vector

Algorithm 1: *SSIC*: Sequential Surveillance with Interference Cancellation

Input: $\boldsymbol{\mathcal{W}}_{\widetilde{\boldsymbol{\theta}}_p}$: Surveillance measurement matrices designed for each sector; $\widehat{\boldsymbol{\theta}}_k$: The estimated position of the currently tracked targets; Γ: threshold.

Output: The decision: $\mathcal{H}$

for $1 \leq p \leq N_S$ **do**

- Take measurements via $\boldsymbol{\mathcal{W}}_{\widetilde{\boldsymbol{\theta}}_p}$:

$$\boldsymbol{y}_p = \boldsymbol{\mathcal{W}}_{\widetilde{\boldsymbol{\theta}}_p} \left(\boldsymbol{x}\left(\boldsymbol{\theta}, s, \boldsymbol{t}\right) + \boldsymbol{n} \right)$$

- Cancel interference from the currently tracked targets:

$$\widehat{\boldsymbol{y}}_p = \boldsymbol{y}_p - \boldsymbol{\mathcal{W}}_{\widetilde{\boldsymbol{\theta}}_p} \left(\sum_{k=1}^{K} \boldsymbol{x}\left(\widehat{\boldsymbol{\theta}}_k, s_j, \boldsymbol{t}\right) \right)$$

- Estimate parameters:

$$\left\{ \widehat{s}, \widehat{\boldsymbol{\theta}} \right\} = \arg\min_{s', \boldsymbol{\theta}'} \left\| \widehat{\boldsymbol{y}}_p - \boldsymbol{\mathcal{W}}_{\widetilde{\boldsymbol{\theta}}_p} \boldsymbol{x}\left(\boldsymbol{\theta}', s', \boldsymbol{t}\right) \right\|$$

- Compute likelihood:

$$\mathcal{L}_p = \frac{P\left(\widehat{\boldsymbol{y}}_p \middle| \boldsymbol{\mathcal{W}}_{\widetilde{\boldsymbol{\theta}}_p} \boldsymbol{x}\left(\widehat{\boldsymbol{\theta}}, \widehat{s}, \boldsymbol{t}\right), \boldsymbol{\Sigma}_{\boldsymbol{p}} \right)}{P\left(\widehat{\boldsymbol{y}}_p \middle| \mathbf{0}, \boldsymbol{\Sigma}_{\boldsymbol{p}} \right)}$$

- For the decision based on:

$$\mathcal{H} = \max_{1 \leq p \leq N_S} \mathcal{L}_p \underset{\mathcal{H}_0}{\overset{\mathcal{H}_1}{\gtrless}} \Gamma$$

return $\mathcal{H}$

of the corresponding sector. By carefully locating the design vectors, as elaborated in Section 3.1.2, robust surveillance performance (by maximizing the worst case performance) is achieved for emerging targets that do not coincide with the design vector.

The major motivations behind Algorithm 1 can be explained as follows: Since the signal to be detected includes unknown parameters, the ML estimation of these parameters is performed first and then the likelihood ratio is constructed based on the estimated parameters. This approach is known as the generalized likelihood ratio test (GLRT) and is commonly employed in the presence of hypotheses with unknown parameters [57]. Another important point in Algorithm 1 is that the decision is performed based on the maximum of the likelihood ratios obtained for different sectors since a target can be located in any segment which is unknown a priori.

3.1.2 Partitioning of Surveillance Space for Sequential Surveillance

In order to provide robust surveillance performance in the compressed domain, for a known sector $\mathcal{S}_p$, $\widetilde{\boldsymbol{\theta}}_p$ can be designated as follows:

$$\widetilde{\boldsymbol{\theta}}_p = \underset{\boldsymbol{\theta} \in \mathcal{S}_p}{\arg\max} \operatorname{Tr}\left\{\boldsymbol{J}^{-1}\left(\boldsymbol{W}_{\boldsymbol{\theta}}, \boldsymbol{\theta}\right)\right\}, \tag{3.1}$$

where $\widetilde{\boldsymbol{\theta}}_p$ is chosen as a vector in the parameter space with the largest CRLB in $\mathcal{S}_p$. Based on this criterion, the motivation is to minimize the worst case performance inside $\mathcal{S}_p$ since $\boldsymbol{W}_{\widetilde{\boldsymbol{\theta}}_p}$ provides the best performance (the lowest CRLB) for $\widetilde{\boldsymbol{\theta}}_p$; that is,

$$\operatorname{Tr}\left\{\boldsymbol{J}^{-1}\left(\boldsymbol{W}_{\widetilde{\boldsymbol{\theta}}_p}, \widetilde{\boldsymbol{\theta}}_p\right)\right\} \geq \operatorname{Tr}\left\{\boldsymbol{J}^{-1}\left(\boldsymbol{W}_{\boldsymbol{\theta}_v}, \widetilde{\boldsymbol{\theta}}_p\right)\right\}, \tag{3.2}$$

where $\widetilde{\boldsymbol{\theta}}_p \neq \boldsymbol{\theta}_v$ and $\operatorname{Tr}\left\{\boldsymbol{J}^{-1}\left(\boldsymbol{W}_{\widetilde{\boldsymbol{\theta}}_p}, \boldsymbol{\theta}_v\right)\right\}$ refers to the CRLB for DOA $\boldsymbol{\theta}_v$ when the measurement matrix $\boldsymbol{W}_{\widetilde{\boldsymbol{\theta}}_p}$ is used.

When sectors are unknown, $\mathcal{S}$ is partitioned so that the worst case performance of all of sectors is minimized. This can be written as the following minmax type optimization problem:

$$\begin{aligned} &\min_{\mathcal{S}_p} \max_{\boldsymbol{\theta} \in \mathcal{S}_p} \operatorname{Tr}\left\{\boldsymbol{J}^{-1}\left(\boldsymbol{W}_{\boldsymbol{\theta}}, \boldsymbol{\theta}\right)\right\} \\ &\text{s.t.} \\ &\quad \mathcal{S}_1 \cup \mathcal{S}_2 \cup .... \cup \mathcal{S}_{N_S} = \mathcal{S} \\ &\quad \mathcal{S}_p \cap \mathcal{S}_v = \emptyset, \ \forall \ p \neq v. \end{aligned} \tag{3.3}$$

Since it is very challenging to obtain a closed-form solution of (3.3), a greedy algorithm is developed, i.e., the proposed partitioning technique converges to a local minimum of (3.3). The proposed partitioning technique is inspired by the vector quantization algorithms, such as K-means [58], where sectors can be considered as clusters, design vectors $\left\{\widetilde{\boldsymbol{\theta}}_1, ..., \widetilde{\boldsymbol{\theta}}_{N_S}\right\}$ correspond to centers, (or, more generally, representation vectors) of clusters and $\operatorname{Tr}\left\{\boldsymbol{J}^{-1}\left(\boldsymbol{W}_{\boldsymbol{\theta}_v}, \widetilde{\boldsymbol{\theta}}_p\right)\right\}$ is the error when vector $\boldsymbol{\theta}_v$ is represented as $\widetilde{\boldsymbol{\theta}}_p$.

Algorithm 2: Partitioning Algorithm for Surveillance

Input: N_S: Number of sectors, N_G: Grid size

Output: $\left\{\widetilde{\boldsymbol{\theta}}_1, ..., \widetilde{\boldsymbol{\theta}}_{N_S}\right\}$: Set of design vectors for each sector, $\left\{\breve{\boldsymbol{\theta}}_1, ..., \breve{\boldsymbol{\theta}}_{N_G}\right\}$: Set of grid vectors on $\mathcal{S}$, $\{I_1, ..., I_{N_G}\}$: Set of indices mapping each grid vector to a sector.

- Generate the training set spanning the parameter space using N_G vectors: $\left\{\breve{\boldsymbol{\theta}}_1, ..., \breve{\boldsymbol{\theta}}_{N_G}\right\}$.
- Initialize design vectors for each sector: $\left\{\widetilde{\boldsymbol{\theta}}_1, ..., \widetilde{\boldsymbol{\theta}}_{N_S}\right\}$
- **while** *convergence is reached* **do**
  - **for** $1 \leq g \leq N_G$ **do**
    - Assign each $\breve{\boldsymbol{\theta}}_g$ to a sector:
      $$I_g = \underset{1 \leq p \leq N_s}{\arg\min} \operatorname{Tr}\left\{\boldsymbol{J}^{-1}\left(\boldsymbol{W}_{\widetilde{\boldsymbol{\theta}}_p}, \breve{\boldsymbol{\theta}}_g\right)\right\}.$$
  - **for** $1 \leq p \leq N_S$ **do**
    - Update design vectors for each sector: :
      $$\widetilde{\boldsymbol{\theta}}_p = \underset{\breve{\boldsymbol{\theta}}_g \ | I_g = p}{\arg\max} \operatorname{Tr}\left\{\boldsymbol{J}^{-1}\left(\boldsymbol{W}_{\widetilde{\boldsymbol{\theta}}_p}, \breve{\boldsymbol{\theta}}_g\right)\right\}$$
- **return** $\left\{\widetilde{\boldsymbol{\theta}}_1, ..., \widetilde{\boldsymbol{\theta}}_{N_S}\right\}$, $\left\{\breve{\boldsymbol{\theta}}_1, ..., \breve{\boldsymbol{\theta}}_{N_G}\right\}$, $\{I_1, ..., I_{N_G}\}$

As summarized in Algorithm 2, the search space is first discretized by a set of N_G grid vectors, $\left\{\breve{\boldsymbol{\theta}}_1, ..., \breve{\boldsymbol{\theta}}_{N_G}\right\}$ and the design vectors are initialized, $\left\{\widetilde{\boldsymbol{\theta}}_1, ..., \widetilde{\boldsymbol{\theta}}_{N_S}\right\}$. Then, each grid vectors is mapped to a sector such that

$$I_g = \underset{1 \leq p \leq N_s}{\arg\min} \operatorname{Tr}\left\{\boldsymbol{J}^{-1}\left(\boldsymbol{W}_{\widetilde{\boldsymbol{\theta}}_p}, \breve{\boldsymbol{\theta}}_g\right)\right\}, \ 1 \leq g \leq N_G, \tag{3.4}$$

where I_g denotes the sector of grid vector $\breve{\boldsymbol{\theta}}_g$. Then, corresponding to the discretized version of (3.1), each design vector is updated as the grid vector with the worst performance:

$$\widetilde{\boldsymbol{\theta}}_p = \underset{\breve{\boldsymbol{\theta}}_g \ | I_g = p}{\arg\max} \operatorname{Tr}\left\{\boldsymbol{J}^{-1}\left(\boldsymbol{W}_{\widetilde{\boldsymbol{\theta}}_p}, \breve{\boldsymbol{\theta}}_g\right)\right\}, \ 1 \leq p \leq N_S. \tag{3.5}$$

By iteratively applying (3.4) and (3.5), the proposed partitioning technique converges to a local minimum. Convergence can be detected if $\left\{\widetilde{\boldsymbol{\theta}}_1, ..., \widetilde{\boldsymbol{\theta}}_{N_S}\right\}$ and $\{I_1, ..., I_{N_G}\}$ do not change in the consecutive iterations.

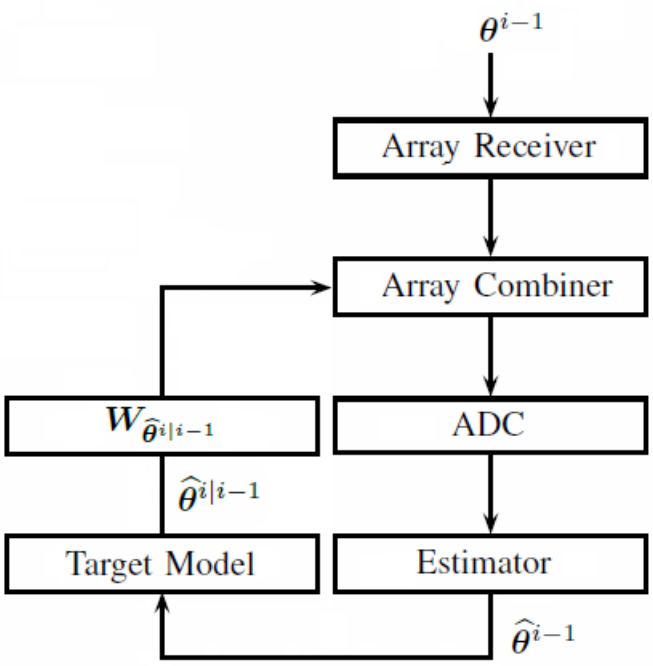

Figure 3.1: Adaptive target tracking by the proposed measurement matrix design algorithm.

3.2 Adaptive Tracking of a Target by Using the Proposed Measurement Matrix Design

Once a newly emerged target is detected in the surveillance mode, the corresponding parameters of the target are passed to the tracker. In the tracking mode the predicted position $\widehat{\boldsymbol{\theta}}^{i|i-1}$ of a tracked target can be obtained by using a proper target model and the past estimates. As demonstrated in Fig. 3.1, the measurement matrix $\boldsymbol{W}_{\widehat{\boldsymbol{\theta}}^{i|i-1}}$ is adaptively designed, e.g., using the approach from Section 2.2, based on the previous estimate of the target position.

Chapter 4

Surveillance and Tracking of Multiple Targets

In this chapter, the proposed techniques for the surveillance and tracking of a single target in Chapter 3 are extended to multiple targets in scene. An algorithm, as referred to as Adaptive Tracking of Multiple Targets using Successive Interference Cancellation (*ATSIC*), is developed in order to successively cancel the interference while adaptively updating the measurement matrices with the proposed technique in Section 2.2. Futhermore, in Section 4.2, a novel technique built upon proposed *ATSIC* and *SSIC* (Section 3.1.1) is introduced so as to jointly perform surveillance and tracking of multiple targets in the scene.

4.1 Adaptive Tracking of Multiple Targets Using Successive Interference Cancellation

The adaptive tracking algorithm for a single target proposed Section 3.2 can be extended to the case of multiple targets by employing successive interference cancellation. As summarized in Algorithm 3, referred to as *ATSIC*, adaptive tracking is performed by eliminating the inference from other currently tracked

Algorithm 3: *ATSIC*: Adaptive Tracking of Multiple Targets using Successive Interference Cancellation

Input: $\widehat{\boldsymbol{\theta}}_k^{[i-1]}$ $(1 \leq k \leq K)$: The predicted position of K targets for $(i-1)^{\text{th}}$ snapshot.

Output: $\widehat{\boldsymbol{\theta}}_k^{[i]}$ $(1 \leq k \leq K)$: The predicted position of K targets for i^{th} snapshot.

for $1 \leq k \leq K$ **do**

- Update current estimate based on state evolution model:

$$\widehat{\boldsymbol{\theta}}_k^{[i|i-1]} = \mathcal{F}_k\left(\widehat{\boldsymbol{\theta}}_k^{[i-1]}\right)$$

- Take measurements via $\boldsymbol{\mathcal{W}}_{\widehat{\boldsymbol{\theta}}_k^{[i|i-1]}}$:

$$\boldsymbol{y}_k^{[i]} = \boldsymbol{\mathcal{W}}_{\widehat{\boldsymbol{\theta}}_k^{[i|i-1]}}\left(\sum_{j=1}^{K} \boldsymbol{x}\left(\boldsymbol{\theta}_j, s_j, \boldsymbol{t}\right) + \boldsymbol{n}\right)$$

- Eliminate interference from other targets:

$$\widehat{\boldsymbol{y}}_k^{[i]} = \boldsymbol{y}_k^{[i]} - \boldsymbol{\mathcal{W}}_{\widehat{\boldsymbol{\theta}}_k^{[i|i-1]}}\left(\sum_{j\neq k}^{K} \boldsymbol{x}\left(\widehat{\boldsymbol{\theta}}_j^{[i|i-1]}, s_j, \boldsymbol{t}\right) + \boldsymbol{n}\right)$$

- Estimate parameters:

$$\widehat{\boldsymbol{\theta}}_k^{[i]} = \arg\min_{\boldsymbol{\theta}} \left\| \widehat{\boldsymbol{y}}_k^{[i]} - \boldsymbol{\mathcal{W}}_{\widehat{\boldsymbol{\theta}}_k^{[i|i-1]}} \boldsymbol{x}\left(\boldsymbol{\theta}, s_k, \boldsymbol{t}\right) \right\|$$

return $\widehat{\boldsymbol{\theta}}_k^{[i]}$ $(1 \leq k \leq K)$

targets. To track each target, measurements can be used as proposed in Section 2.2, and before performing tracking, the interference from the other targets can be cancelled out using the previous estimates.

4.2 Joint Operation of Surveillance and Tracking

To comprehensively perform joint operation of surveillance and tracking, the previously proposed methods are combined, where the positions of currently tracked targets are first estimated via the *ATSIC* algorithm and the surveillance is conducted using *SSIC* as illustrated in Algorithm 4.

In Algorithm 4, the DoAs of (actively) tracked targets for the current snapshot are first estimated by using *ATSIC* algorithm. Then, the estimated DoAs are

Algorithm 4: Joint Operation of Tracking and Surveillance

Input: $K^{[i-1]}$: The number of tracked targets at $(i-1)^{\text{th}}$ snapshot, $\widehat{\boldsymbol{\theta}}_k^{[i-1]}$ $(1 \leq k \leq K)$: The predicted position of K targets for $(i-1)^{\text{th}}$ snapshot, $\boldsymbol{\mathcal{W}}_{\widetilde{\boldsymbol{\theta}}_p}$: Surveillance measurement matrices designed for each sector, Γ: likelihood threshold.

Output: $K^{[i]}$: The number of tracked targets at i^{th} snapshot, $\widehat{\boldsymbol{\theta}}_k^{[i]}$ $(1 \leq k \leq K)$: The predicted position of K targets for i^{th} snapshot.

1. Estimate the current position of targets in the scene using *ATSIC*:
   $\widehat{\boldsymbol{\theta}}_k^{[i]} = ATSIC\left(\widehat{\boldsymbol{\theta}}_k^{[i-1]}\right)$ $(1 \leq k \leq K)$
2. Perform surveillance using *SSIC*:
   if SSIC $\left(\widehat{\boldsymbol{\theta}}_k^{[i]}, \boldsymbol{\mathcal{W}}_{\widetilde{\boldsymbol{\theta}}_p}, \Gamma\right)$ **then**
   $K^{[i]} = K^{[i-1]} + 1$

return $K^{[i]}$ *and* $\widehat{\boldsymbol{\theta}}_k^{[i]}$

passed to *SSIC* algorithm, which uses the estimated DoAs in order to cancel out the interference caused by them in the measurements. Then, *SSIC* algorithm performs surveillance as discussed in detail in Section 3.1.1. If a newly emerging target is detected, then its initial DoA estimate is passed to *ATSIC* algorithm and it is tracked *ATSIC* in the next snapshots.

Chapter 5

The Performance of the Proposed Measurement Matrix Design for Surveillance and Tracking

In this chapter, the surveillance and tracking performance of the proposed techniques are evaluated and compared via a comprehensive set of simulations. In Section 5.1, the performance of the proposed and Gaussian matrices are illustrated as a function of elevation and Signal-to-Noise (SNR). In Section 5.2, the sensitivity analysis of the proposed measurement matrices are performed and compared with Gaussian matrices in the case of perturbation in the design vector and unknown complex amplitude. In Section 5.3.1, the performance of the partitonining technique introduced in Section 3.1.2 is discussed. In Section 5.3.2, the Receiver Operating Characteristics (ROC) of *SSIC* is performed. The performance of proposed adaptive tracking technique is discussed in Section 5.4. Finally, the performance of *ATSIC* is illustrated in Section 5.5.

5.1 Performance of the Proposed Measurement Matrix Design Algorithm

To evaluate performance of the proposed measurement matrix design technique, $N = 24$ sensors are compressed to $M = 2$ outputs. A uniform circular array (UCA) alignment is used so that the sensor array becomes equally sensitive to all ϕ angles and $\mathrm{Tr}\left\{\boldsymbol{J}^{-1}\left(\boldsymbol{W},\boldsymbol{\theta}\right)\right\}$ is a function of γ and $\boldsymbol{W}$ only. For various values of γ spanning from 0 to $\frac{\pi}{2}$, target DoA, represented as $\boldsymbol{\theta}_0$, is estimated based on measurements captured through two types of measurement matrices; the proposed measurement matrix designed for $\boldsymbol{\theta}_0$ denoted as $\boldsymbol{W}_{\boldsymbol{\theta}_0}$ and the random Gaussian matrix whose entries are independently taken from circularly symmetric complex normal distribution, denoted as $\boldsymbol{W}_R$. After acquiring measurements via $\boldsymbol{W}_{\boldsymbol{\theta}_0}$, the parameter of interest $\boldsymbol{\theta}_0$ is estimated using gradient descent techniques as

$$\widehat{\boldsymbol{\theta}_0} = \arg\min_{\boldsymbol{\theta}'} \left\|\boldsymbol{y} - \boldsymbol{\mathcal{W}}_{\boldsymbol{\theta}_0}\boldsymbol{x}\left(\boldsymbol{\theta}', s, \boldsymbol{t}\right)\right\|. \tag{5.1}$$

To measure performance using random matrices, $\boldsymbol{\mathcal{W}}_{\boldsymbol{\theta}_0}$ is replaced in (5.1) with $\boldsymbol{\mathcal{W}}_R$.

For the results presented in this part, measurement matrix $\boldsymbol{W}$ is designed on the actual DoA of a target ($\boldsymbol{\theta}_0$), i.e., $\boldsymbol{W}_{\boldsymbol{\theta}_0}$ is used to capture measurements from a target with DOA $\boldsymbol{\theta}_0$. In Section 5.2, the case in which measurement matrix $\boldsymbol{W}$ is designed for a general $\boldsymbol{\theta}$ where $\boldsymbol{\theta}_0$ is not equal to $\boldsymbol{\theta}$ is also analyzed. The estimation accuracy of DoA is assessed by the root-mean-squared error (RMSE), which is given by

$$\mathrm{e}_{RMS}\left(\boldsymbol{W}_{\boldsymbol{\theta}_0}, \boldsymbol{\theta}_0\right) = \frac{180}{\pi}\sqrt{\mathrm{E}_{\boldsymbol{n}}\left\{\left(\gamma_0 - \widehat{\gamma}_0\right)^2 + \left(\phi_0 - \widehat{\phi}_0\right)^2\right\}}, \tag{5.2}$$

where $\mathrm{e}_{RMS}\left(\boldsymbol{W}, \boldsymbol{\theta}_0\right)$ refers to the RMSE when $\boldsymbol{W}$ is used a measurement matrix, and $\widehat{\theta}$ and $\widehat{\phi}$ are estimates of θ and ϕ using (5.1), respectively. Expectation in (5.2) is computed over $\boldsymbol{n}$ as defined in (2.6). Note that $\mathrm{e}_{RMS}\left(\boldsymbol{W}, \boldsymbol{\theta}\right)$ includes errors related to both elevation and azimuth.

In Fig. 5.1, $\mathrm{e}_{RMS}(\boldsymbol{W}_{\boldsymbol{\theta}_0}, \boldsymbol{\theta}_0)$ and $\mathrm{e}_{RMS}(\boldsymbol{W}_R, \boldsymbol{\theta}_0)$ are demonstrated for a signal-to-noise ratio (SNR) of 3 dB, where SNR is defined as $\frac{|s|^2}{\sigma_n^2}$, and the square root of $\mathrm{Tr}\left\{\boldsymbol{J}^{-1}(\boldsymbol{W}_{\boldsymbol{\theta}_0}, \boldsymbol{\theta}_0)\right\}$ is plotted as a function of γ. It is observed that the proposed measurement design technique provides lower RMSEs for all γ_0. On average, the proposed matrix $\boldsymbol{W}_{\boldsymbol{\theta}_0}$ yields 0.43 of the RMSE error achieved by $\boldsymbol{W}_R$, the random Gaussian matrix. The proposed $\boldsymbol{W}_{\boldsymbol{\theta}_0}$ yields performance enhancements over $\boldsymbol{W}_R$ especially for smaller values of $0^o < \gamma_0 \leq 15^o$ and higher values of $75^o \leq \gamma_0 < 90^o$, where it provides considerable enhancements over the estimation of γ and ϕ, respectively.

The individual CRLBs provided by the proposed measurement design technique for elevation and azimuth can be computed the following

$$e_\gamma(\boldsymbol{W}_{\boldsymbol{\theta}_0}, \boldsymbol{\theta}_0) = \frac{J_\gamma(\boldsymbol{W}_{\boldsymbol{\theta}_0}, \boldsymbol{\theta}_0)}{J_\gamma(\boldsymbol{W}_{\boldsymbol{\theta}_0}, \boldsymbol{\theta}_0) J_\phi(\boldsymbol{W}_{\boldsymbol{\theta}_0}, \boldsymbol{\theta}_0) - \left(J_{\gamma\phi}(\boldsymbol{W}_{\boldsymbol{\theta}_0}, \boldsymbol{\theta}_0)\right)^2} \tag{5.3}$$

$$e_\phi(\boldsymbol{W}_{\boldsymbol{\theta}_0}, \boldsymbol{\theta}_0) = \frac{J_\phi(\boldsymbol{W}_{\boldsymbol{\theta}_0}, \boldsymbol{\theta}_0)}{J_\phi(\boldsymbol{W}_{\boldsymbol{\theta}_0}, \boldsymbol{\theta}_0) J_\phi(\boldsymbol{W}_{\boldsymbol{\theta}_0}, \boldsymbol{\theta}_0) - \left(J_{\gamma\phi}(\boldsymbol{W}_{\boldsymbol{\theta}_0}, \boldsymbol{\theta}_0)\right)^2}, \tag{5.4}$$

where $e_\gamma(\boldsymbol{W}_{\boldsymbol{\theta}_0}, \boldsymbol{\theta}_0)$ and $e_\phi(\boldsymbol{W}_{\boldsymbol{\theta}_0}, \boldsymbol{\theta}_0)$ correspond to the CRLB for elevation and azimuth, respectively.

In Fig. 5.2, the RMSE version of $e_\gamma(\boldsymbol{W}_{\boldsymbol{\theta}_0}, \boldsymbol{\theta}_0)$ and $e_\phi(\boldsymbol{W}_{\boldsymbol{\theta}_0}, \boldsymbol{\theta}_0)$ are shown as a function of γ. It is observed that the performance for elevation degrades with the higher values of elevation whereas the performance for azimuth enhances with the higher values of elevation. Moreover, the proposed measurement design technique yields equivalent performance for elevation and azimuth. $e_\gamma(\boldsymbol{W}_{\boldsymbol{\theta}_0}, \boldsymbol{\theta}_0)$ and $e_\phi(\boldsymbol{W}_{\boldsymbol{\theta}_0}, \boldsymbol{\theta}_0)$ are symmetric with $\gamma_0 = 45^0$ and equal when $\gamma_0 = 45^0$.

In Fig. 5.3, $\mathrm{E}_{\boldsymbol{\theta}_0}\left\{\mathrm{e}_{RMS}(\boldsymbol{W}_{\boldsymbol{\theta}_0}, \boldsymbol{\theta}_0)\right\}$ and $\mathrm{E}_{\boldsymbol{\theta}_0}\left\{\mathrm{e}_{RMS}(\boldsymbol{W}_R, \boldsymbol{\theta}_0)\right\}$ are illustrated as a function of the SNR, where $\mathrm{E}_{\boldsymbol{\theta}_0}\left\{\mathrm{e}_{RMS}(\boldsymbol{W}_{\boldsymbol{\theta}_0}, \boldsymbol{\theta}_0)\right\}$ and $\mathrm{E}_{\boldsymbol{\theta}_0}\left\{\mathrm{e}_{RMS}(\boldsymbol{W}_R, \boldsymbol{\theta}_0)\right\}$ correspond to average performances over the parameter space $\mathcal{S} = [0,\ \frac{\pi}{2}] \times [0,\ \pi]$ for the proposed and Gaussian measurement matrices, respectively. To compute the average, it is assumed that γ_0 is uniformly distributed over 0 to $\frac{\pi}{2}$ and ϕ_0 is uniformly distributed over 0 to π. The averaged CRLB of the proposed design technique is also indicated and represented as $\mathrm{E}_{\boldsymbol{\theta}_0}\left\{\frac{180}{\pi}\sqrt{\mathrm{Tr}\left\{\boldsymbol{J}^{-1}(\boldsymbol{W}_{\boldsymbol{\theta}_0}, \boldsymbol{\theta}_0)\right\}}\right\}$. The observations imply that while the proposed measurement matrices yield lower

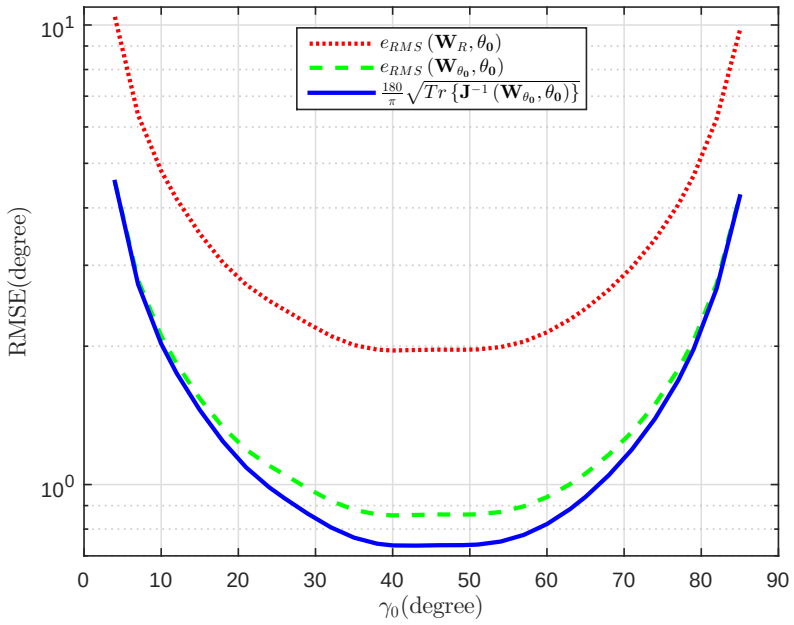

Figure 5.1: The RMSE for DoA estimation as function of γ with the proposed measurement matrix design (green) and its corresponding CRLB (blue) vs RMSE for random Gaussian matrices (red).

RMSE values compared to $\boldsymbol{W}_R$ for SNR values greater than 5dB, it is also seen that the gradient descent estimation for DoA reaches the CRLB level of $\boldsymbol{W}_{\boldsymbol{\theta}_0}$ at SNR's above 20dB. It is observed that the approach of using random Gaussian measurement matrices can never achieve the error performance of using the proposed design matrix $\boldsymbol{W}_{\boldsymbol{\theta}_0}$ for all SNRs and the proposed $\boldsymbol{W}_{\boldsymbol{\theta}_0}$ in average obtains 0.32 of the RMSE $\boldsymbol{W}_R$ reaches. In addition, $\boldsymbol{W}_{\boldsymbol{\theta}_0}$ has the same error level as $\boldsymbol{W}_R$ by requiring around 15dB less SNR.

5.2 Sensitivity Analysis of The Proposed Measurement Matrix Design Algorithm

In the previous simulation results, the proposed measurement matrix is implicitly designed on the target DoA $\boldsymbol{\theta}_0$, i.e., $\boldsymbol{W}_{\boldsymbol{\theta}_0}$ is used to capture measurements from $\boldsymbol{x}(\boldsymbol{\theta}_0, s, \boldsymbol{t})$. Nevertheless, in the majority of the cases, there can exist a

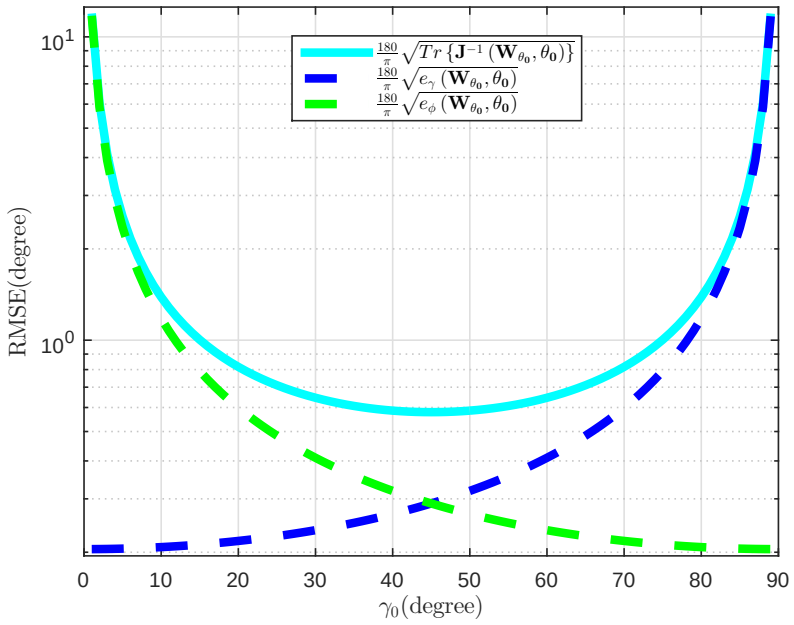

Figure 5.2: The RMSE version of the CRLB for elevation ($e_\gamma(\boldsymbol{W}_{\boldsymbol{\theta}_0},\boldsymbol{\theta}_0)$) (blue), the RMSE version of the CLRB for azimuth ($e_\phi(\boldsymbol{W}_{\boldsymbol{\theta}_0})$) (green) and the RMSE of the total error corresponding to Tr $\{\boldsymbol{J}^{-1}(\boldsymbol{W}_{\boldsymbol{\theta}_0},\boldsymbol{\theta}_0)\} = e_\gamma(\boldsymbol{W}_{\boldsymbol{\theta}_0},\boldsymbol{\theta}_0) + e_\phi(\boldsymbol{W}_{\boldsymbol{\theta}_0},\boldsymbol{\theta}_0)$ (cyan).

certain difference between the vector of design and the true DoA. To represent this situation, the following model is employed

$$\begin{aligned} \boldsymbol{\theta}_0 &= \boldsymbol{\theta}_D + \boldsymbol{\delta}_{\boldsymbol{\theta}} \\ \begin{bmatrix} \gamma_0 \\ \phi_0 \end{bmatrix} &= \begin{bmatrix} \gamma_D \\ \phi_D \end{bmatrix} + \begin{bmatrix} \delta\gamma \\ \delta\phi \end{bmatrix}, \end{aligned} \tag{5.5}$$

where $\boldsymbol{\theta}_0$ is the true DoA, $\boldsymbol{\theta}_D$ represents a known vector of design and $\boldsymbol{\delta}_{\boldsymbol{\theta}} = [\delta\gamma\ \delta\phi]$ is an unknown perturbation parameter.

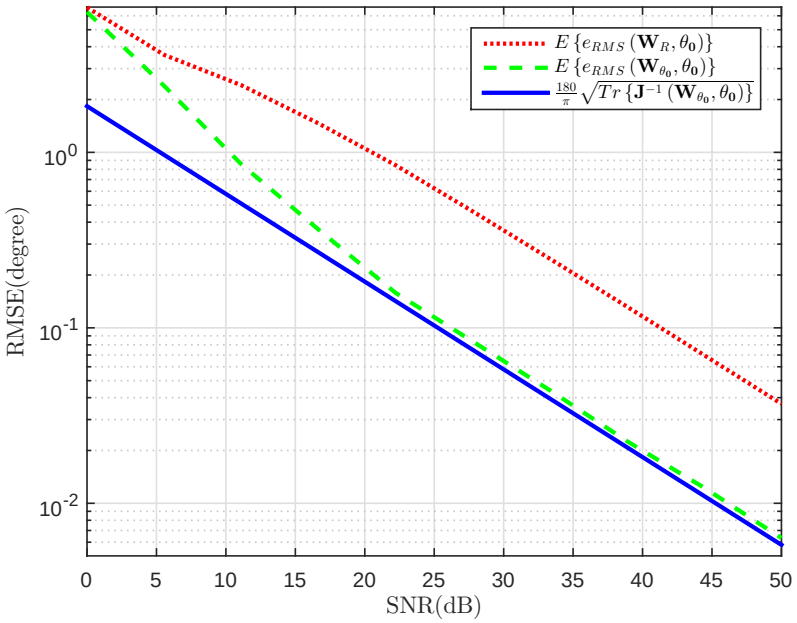

Figure 5.3: The averaged RMSE over parameter space as a function of SNR with the proposed measurement matrix design (green) and its corresponding CRLB (blue) vs the RMSE for random Gaussian matrices (red).

5.2.1 Sensitivity Analysis of The Proposed Measurement Matrix Design Algorithm as a Function of Perturbation in Elevation and Azimuth

The sensitivity of the proposed measurement design technique to perturbations in elevation and azimuth angle is measured when $\boldsymbol{W_\theta}$ is utilized measurement matrix and the DoA is $\boldsymbol{\theta}_0$. Then, the CRLB depends on both $\boldsymbol{\theta}_D$ and $\delta\boldsymbol{\theta}$ and can be written as

$$\mathrm{Tr}\left\{\boldsymbol{J}\left(\boldsymbol{W}_{\boldsymbol{\theta}_D}, \boldsymbol{\theta}_D, \boldsymbol{\delta}_{\boldsymbol{\theta}}\right)\right\} = \frac{J_\gamma\left(\boldsymbol{W}_{\boldsymbol{\theta}_D}, \boldsymbol{\theta}_D + \boldsymbol{\delta\theta}\right) + J_\phi\left(\boldsymbol{W}_{\boldsymbol{\theta}_D}, \boldsymbol{\theta}_D + \boldsymbol{\delta\theta}\right)}{J_\gamma\left(\boldsymbol{W}_{\boldsymbol{\theta}_D}, \boldsymbol{\theta}_D + \boldsymbol{\delta\theta}\right) J_\phi\left(\boldsymbol{W}_{\boldsymbol{\theta}_D}, \boldsymbol{\theta}_D + \boldsymbol{\delta\theta}\right) - \left(J_{\gamma\phi}\left(\boldsymbol{W}_{\boldsymbol{\theta}_D}, \boldsymbol{\theta}_D + \boldsymbol{\delta\theta}\right)\right)^2}. \tag{5.6}$$

In Fig. 5.4, RMSE version of the averaged CRLB over design vector on the parameter space, i.e., $\frac{180}{\pi}\sqrt{\mathrm{E}_{\boldsymbol{\theta}_D}\left\{\mathrm{Tr}\left\{\boldsymbol{J}\left(\boldsymbol{W}_{\boldsymbol{\theta}_D}, \boldsymbol{\theta}_D, \boldsymbol{\delta}_{\boldsymbol{\theta}}\right)\right\}\right\}}$, is illustrated as a function of $\delta\gamma$ and $\delta\phi$. In Fig. 5.4, the performance of the proposed measurement design

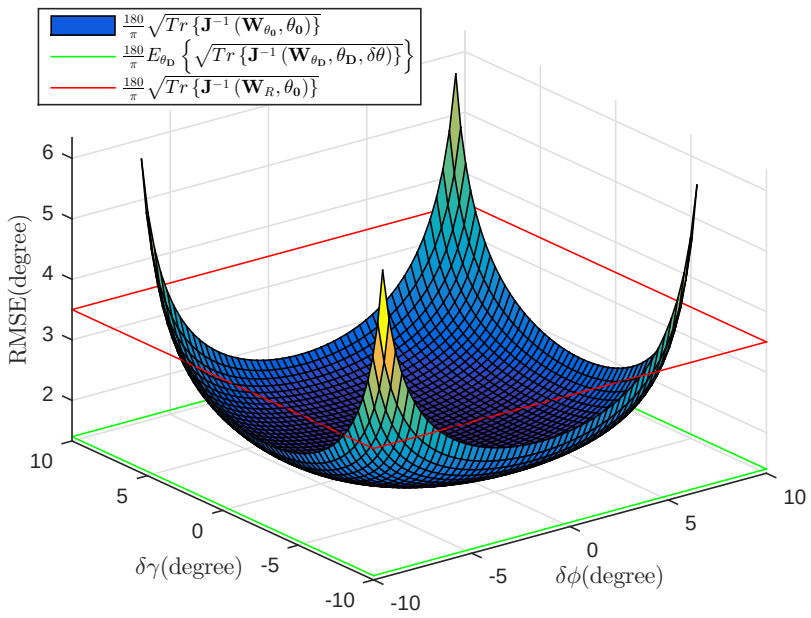

Figure 5.4: The RMSE version of the CRLB computed by the proposed measurement matrix design in the case of perturbation in elevation and azimuth angle of design.

technique under not perturbation in the design vector and the performance of random matrices are also demonstrated that are denoted by $\frac{180}{\pi}\sqrt{\mathrm{Tr}\left\{\boldsymbol{J}\left(\boldsymbol{W}_{\boldsymbol{\theta}_0}\right\},\boldsymbol{\theta}_0,\right)}$ and $\frac{180}{\pi}\sqrt{\mathrm{Tr}\left\{\boldsymbol{J}\left(\boldsymbol{W}_R,\boldsymbol{\theta}_0,\right)\right\}}$, respectively. $\frac{180}{\pi}\sqrt{\mathrm{Tr}\left\{\boldsymbol{J}\left(\boldsymbol{W}_{\boldsymbol{\theta}_0},\boldsymbol{\theta}_0,\right)\right\}}$ provides a lower-bound to $\frac{180}{\pi}\sqrt{\mathrm{E}_{\boldsymbol{\theta}_D}\left\{\mathrm{Tr}\left\{\boldsymbol{J}\left(\boldsymbol{W}_{\boldsymbol{\theta}_D},\boldsymbol{\theta}_D,\boldsymbol{\delta}_{\boldsymbol{\theta}}\right)\right\}\right\}}$, as expected. The circular contours of $\frac{180}{\pi}\sqrt{\mathrm{E}_{\boldsymbol{\theta}_D}\left\{\mathrm{Tr}\left\{\boldsymbol{J}\left(\boldsymbol{W}_{\boldsymbol{\theta}_D},\boldsymbol{\theta}_D,\boldsymbol{\delta}_{\boldsymbol{\theta}}\right)\right\}\right\}}$ illustrates that the proposed technique is equally sensitive to perturbation in elevation and azimuth. In other words, the degradation of performance due to perturbation in elevation and azimuth are equal when $\delta\gamma = \delta\phi$. Another observation is that the proposed measurement design technique enhances the performance of random measurement matrices when $|\delta\gamma| \leq 5.72^o$ and $|\delta\phi| \leq 5.72^o$.

5.2.2 Sensitivity Analysis of The Proposed Measurement Matrix Design Algorithm In The Case of Random Perturbation

In order to analyze the sensitivity of the proposed design approach to random perturbation from the actual target DoA, consider an i.i.d Gaussian error model denoted by $\boldsymbol{\delta_\theta} \sim \mathcal{N}(\mathbf{0}, \sigma_m^2 \boldsymbol{I})$, The averaged RMSE in the presence of the uncertainty parameter $\boldsymbol{\delta_\theta}$ with standard deviation σ_m is represented as $\mathrm{e}_{RMS}(\boldsymbol{W}_{\boldsymbol{\theta}_D}, \boldsymbol{\theta}_0, \sigma_m)$. Then, the sensitivity of our proposed measurement design technique can be associated with $\mathrm{E}_{\boldsymbol{\delta_\theta}}\{\mathrm{E}_{\boldsymbol{\theta}_0}\{\mathrm{e}_{RMS}(\boldsymbol{W}_{\boldsymbol{\theta}_D}, \boldsymbol{\theta}_0, \sigma_m)\}\}$, where the inner expectation is carried out over $\boldsymbol{\theta}_0$ and the outer expectation is taken over $\delta_{\boldsymbol{\theta}}$.

In Fig. 5.5, $\mathrm{E}_{\boldsymbol{\delta_\theta}}\{\mathrm{E}_{\boldsymbol{\theta}_0}\{\mathrm{e}_{RMS}(\boldsymbol{W}_{\boldsymbol{\theta}_D}, \boldsymbol{\theta}_0, \sigma_m)\}\}$ is demonstrated as a function of standard deviation σ_m, with $\mathrm{E}_{\boldsymbol{\delta_\theta}}\{\mathrm{E}_{\boldsymbol{\theta}_0}\{\mathrm{e}_{RMS}(\boldsymbol{W}_{\boldsymbol{\theta}_D}, \boldsymbol{\theta}_0, 0)\}\}$ denoting the averaged RMSE under no uncertainty, i.e., $\sigma_m = 0$ and $\mathrm{E}_{\boldsymbol{\theta}_0}\{\mathrm{e}_{RMS}(\boldsymbol{W}_R, \boldsymbol{\theta}_0)\}$ representing the averaged RMSE for the random matrices approach, which is insensitive to any model uncertainty. It is observed that the proposed technique is quite robust against uncertainties in the sense that the performance degrades slowly as σ_m increases. In particular, the proposed technique outperforms the random matrices approach for $\sigma_m \leq 7.3^o$ in average, which is a very wide interval in practice for the standard deviation of the perturbation term. In other words, it is possible to obtain more accurate results via the proposed technique if the information on $\boldsymbol{\theta}$ is available with less than 7.3^o RMSE in $\boldsymbol{\theta}$. Such information can be available based on previous estimates and/or prior information in practical systems.

5.2.3 Sensitivity Analysis of The Proposed Measurement Matrix Design Algorithm In The Case of Unknown Complex Amplitude

In the previous simulations, it is assumed that s (complex amplitude) is known or it is estimated in Algorithm 1 with neglectfully small error. To assess the

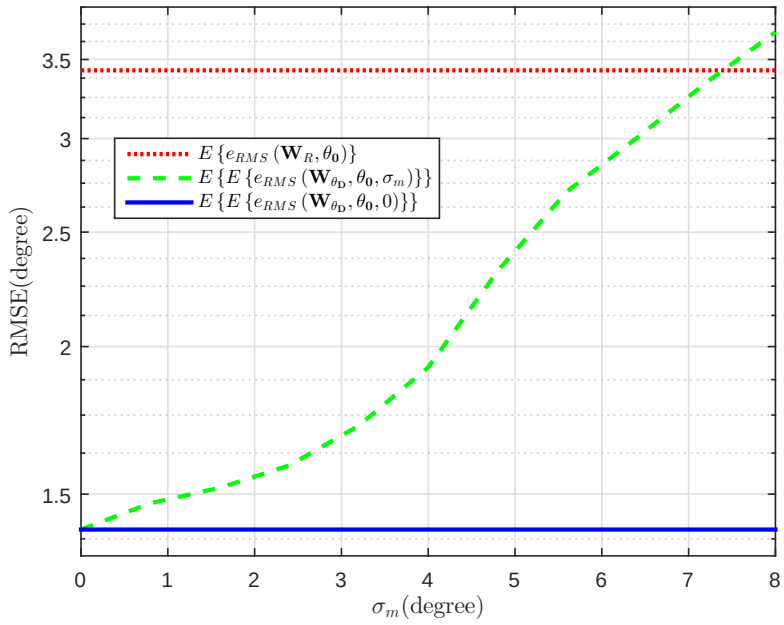

Figure 5.5: The averaged RMSE error over parameter space for DoA estimation with the proposed measurement matrices as function of the standard deviation (σ_m) in the design vector ($\boldsymbol{\theta}_D$) (green), the averaged RMSE under no perturbation (blue), the averaged RMSE of Gaussian matrices (red).

performance of the proposed measurement matrices, in the case of unknown s, let s be in the following form:

$$s = s_D \delta_s e^{j(\beta_D + \delta_\beta)}, \tag{5.7}$$

where s_D and β_D are known before designing measurement matrices but the $\delta_{s_n} \in \mathbb{R}^+$ and $\delta_\beta \in \left[-\frac{\pi}{2}\ \frac{\pi}{2}\right]$ are unknown, that are corresponding to unknown magnitude and phase in s, respectively.

Suppose that $\boldsymbol{\theta}_0 = \boldsymbol{\theta}_D + \boldsymbol{\delta}_{\boldsymbol{\theta}}$ as in (5.5) and $\boldsymbol{W}_{\boldsymbol{\theta}_D}$ ($\boldsymbol{\mathcal{W}}_{\boldsymbol{\theta}_D}$) is employed to obtain the measurements as the following

$$\begin{aligned} \boldsymbol{y} &= \boldsymbol{\mathcal{W}}_{\boldsymbol{\theta}_D}\left(\boldsymbol{x}\left(\boldsymbol{\theta}_0', s, \boldsymbol{t}\right) + \boldsymbol{n}\right) \\ &= \left(\boldsymbol{W}_{\boldsymbol{\theta}_D} \otimes \boldsymbol{I}\right)\left(\left(s_D \delta_s e^{j(\beta_D + \delta_\beta)}\right)\left(e^{j\omega \boldsymbol{t}} \otimes e^{j\omega \boldsymbol{\tau}(\boldsymbol{\theta}_D + \boldsymbol{\delta}_{\boldsymbol{\theta}})}\right) + \boldsymbol{n}\right). \end{aligned} \tag{5.8}$$

Then, the error function defined in (5.2) becomes the function of $\boldsymbol{W}_{\boldsymbol{\theta}_D}$, $\boldsymbol{\theta}_0$, $\boldsymbol{\delta}_{\boldsymbol{\theta}}$, δ_β and δ_s, denoted as $\mathrm{e}_{RMS}(\boldsymbol{W}_{\boldsymbol{\theta}_D}, \boldsymbol{\theta}_0, \boldsymbol{\delta}_{\boldsymbol{\theta}}, \delta_\beta, \delta_s)$, where γ and ϕ are estimated by using (5.1) via the measurements as in (5.8).

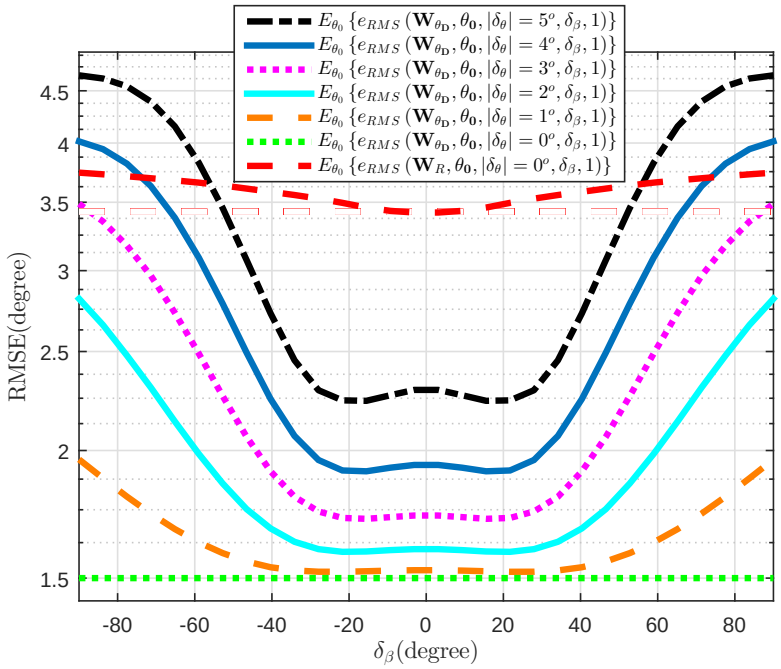

Figure 5.6: The averaged RMSE over parameter space as a function of unknown phase of the complex amplitude (δ_β) for various levels of the perturbation in the design vector ($\boldsymbol{\delta_\theta}$) with the proposed measurement design technique and average RMSE for random matrices.

In Fig. 5.6, the average of $\mathrm{e}_{RMS}(\boldsymbol{W}_{\boldsymbol{\theta}_0}, \boldsymbol{\theta}_0, \boldsymbol{\delta_\theta}, \delta_\beta, \delta_s)$ over $\boldsymbol{\theta}_D$ is illustrated for different values of $\boldsymbol{\delta_\theta}$ spanning from 0^o to 5^o when the magnitude of s is known, i.e., $\delta_s = 1$. $\mathrm{E}_{\boldsymbol{\theta}_0}\{\mathrm{e}_{RMS}(\boldsymbol{W}_R, \boldsymbol{\theta}_0)\}$ is also shown In Fig. 5.6 for comparison. It is observed that the proposed design technique performs better than random measurement matrices for any value of δ_β if $\boldsymbol{\delta} < \mathbf{3}^o$. When $\boldsymbol{\delta} = \mathbf{4}^o$ and $\boldsymbol{\delta} = \mathbf{5}^o$, proposed algorithm has better performance if $|\delta_\beta| \leq 65^o$ and $|\delta_\beta| \leq 52^o$, respectively. Hence, if δ_β is completely unknown, e.g., $\delta_\beta \sim U\,[0\ pi]$, then the proposed technique guarantees performance improvements over random matrices if $\frac{180}{\pi}\sqrt{|\gamma - \widehat{\gamma}|} \leq 3$ and $\frac{180}{\pi}\sqrt{\left|\phi - \widehat{\phi}\right|} \leq 3$.

In Fig. 5.7, the averaged $\mathrm{e}_{RMS}(\boldsymbol{W}_{\boldsymbol{\theta}_D}, \boldsymbol{\theta}_0, \boldsymbol{\delta_\theta}, \delta_\beta, \delta_s)$ over parameter space is demonstrated as a function of $\boldsymbol{\delta_\theta}$ and δ_β when $\delta_s = 1$. As expected, the bottom of $\mathrm{e}_{RMS}(\boldsymbol{W}_{\boldsymbol{\theta}_D}, \boldsymbol{\theta}_0, \boldsymbol{\delta_\theta}, \delta_\beta, 1)$ is $\mathrm{e}_{RMS}(\boldsymbol{W}_{\boldsymbol{\theta}_D}, \boldsymbol{\theta}_0, 0, 0, 1)$ corresponding to the performance of the proposed technique when the complex amplitude is known without any perturbation in the design vector. As contour lines on

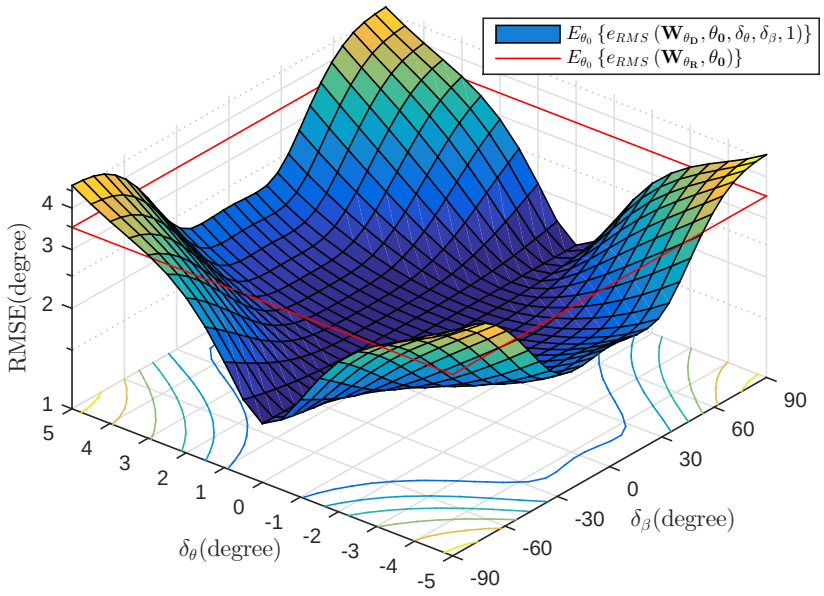

Figure 5.7: The averaged RMSE over parameter space as a function of unknown phase of the complex amplitude (δ_β) and perturbation in the design vector ($\boldsymbol{\delta_\theta}$) with the proposed measurement design technique.

$\mathrm{E}_{\boldsymbol{\theta}_0}\{\mathrm{e}_{RMS}(\boldsymbol{W}_{\boldsymbol{\theta}_D},\boldsymbol{\theta}_0,\boldsymbol{\delta_\theta},\delta_\beta,1)\}$ indicates, $\boldsymbol{\delta_\theta}$ has more impact on performance degradation compared to δ_β.

In Fig. 5.8, Fig. 5.9 and Fig. 5.10, the performance of the proposed measurement matrices in the case of unknown complex magnitude and phase is demonstrated for $\boldsymbol{\delta_\theta} = \mathbf{5}^0$, $\boldsymbol{\delta_\theta} = \mathbf{3}^0$ and $\boldsymbol{\delta_\theta} = \mathbf{1}^0$, respectively. It is observed that as the perturbation in design vector gets smaller, the proposed technique becomes more robust against unknown magnitude and phase, i.e., the bottom plateau of $\mathrm{E}_{\boldsymbol{\theta}_0}\{\mathrm{e}_{RMS}(\boldsymbol{W}_{\boldsymbol{\theta}_D},\boldsymbol{\theta}_0,\boldsymbol{\delta_\theta},\delta_\beta,\delta_s)\}$ broadens for smaller values of $\boldsymbol{\delta_\theta}$. As the contour lines of $\mathrm{E}_{\boldsymbol{\theta}_0}\{\mathrm{e}_{RMS}(\boldsymbol{W}_{\boldsymbol{\theta}_D},\boldsymbol{\theta}_0,\boldsymbol{\delta_\theta},\delta_\beta,\delta_s)\}$ indicates, unknown magnitude has more impact on the performance compared to unknown phase in s. Another observation is that when $\frac{180}{\pi}\sqrt{|\gamma-\widehat{\gamma}|} \leq 3$ and $\frac{180}{\pi}\sqrt{\left|\phi-\widehat{\phi}\right|} \leq 3$, the proposed technique provides better performance than random matrices for any value of complex magnitude and phase, where $\mathrm{E}_{\boldsymbol{\theta}_0}\{\mathrm{e}_{RMS}(\boldsymbol{W}_R,\boldsymbol{\theta}_0,0,0,1)\} = 3.49$.

To investigate the SNR range where the proposed measurement matrices are

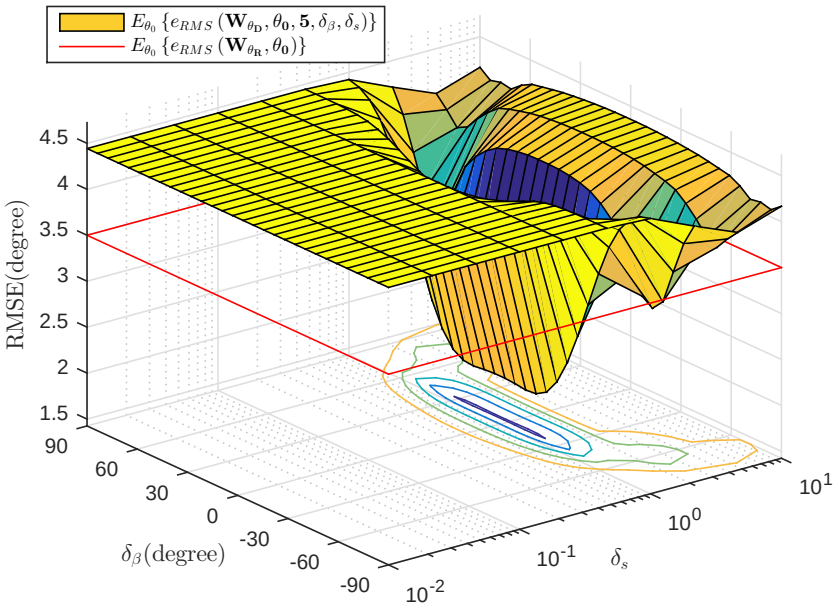

Figure 5.8: The averaged RMSE over parameter space of the proposed measurement matrices in the chase of unknown complex magnitude and phase for $\mathbf{5}^o$ perturbation level ($\boldsymbol{\delta_\theta} = \mathbf{5}^o$).

favorable upon Gaussian matrices, the following scenario is considered. Suppose that a newly emerging target emerging in the scene with DoA $\boldsymbol{\theta}_0$. The complex amplitude of the target is s as in (5.7), where δ_β and δ_s are uniformly distributed random variables over the range of $\left[\frac{-\pi}{2}\ \frac{\pi}{2}\right]$ and $[-1.5\ 1.5]$, respectively. The target is detected by using *SSIC* with the complex amplitude estimate $\widehat{s}$ and the initial DoA estimate $\widehat{\boldsymbol{\theta}}$. Then, at the next snapshot, estimation can be performed as the following

$$\widehat{\boldsymbol{\theta}}_0 = \arg\min_{\boldsymbol{\theta}'} \left\| \boldsymbol{y} - \boldsymbol{\mathcal{W}}_{\widehat{\boldsymbol{\theta}}} \boldsymbol{x}\left(\boldsymbol{\theta}', \widehat{s}, \boldsymbol{t}\right) \right\|, \tag{5.9}$$

where the measurements are captured via $\boldsymbol{\mathcal{W}}_{\widehat{\boldsymbol{\theta}}}$ as $\boldsymbol{y} = \boldsymbol{\mathcal{W}}_{\widehat{\boldsymbol{\theta}}} \boldsymbol{x}\left(\boldsymbol{\theta}_0, s, \boldsymbol{t}\right)$.

In Fig. 5.11, the histogram of the averaged difference in the magnitude of s and $\widehat{s}$ over parameter space, represented as $\mathrm{E}_{\boldsymbol{\theta}_0}\{|s| - |\widehat{s}|\}$, that is acquired by using *SSIC* with 6 sectors as partitioned in Fig. 5.14 is illustrated at different levels of SNR. Similarly, the histogram of the averaged difference in the the phase, denoted as $\mathrm{E}_{\boldsymbol{\theta}_0}\{\angle(s) - \angle(\widehat{s})\}$, is demonstrated in Fig. 5.12. As expected, the

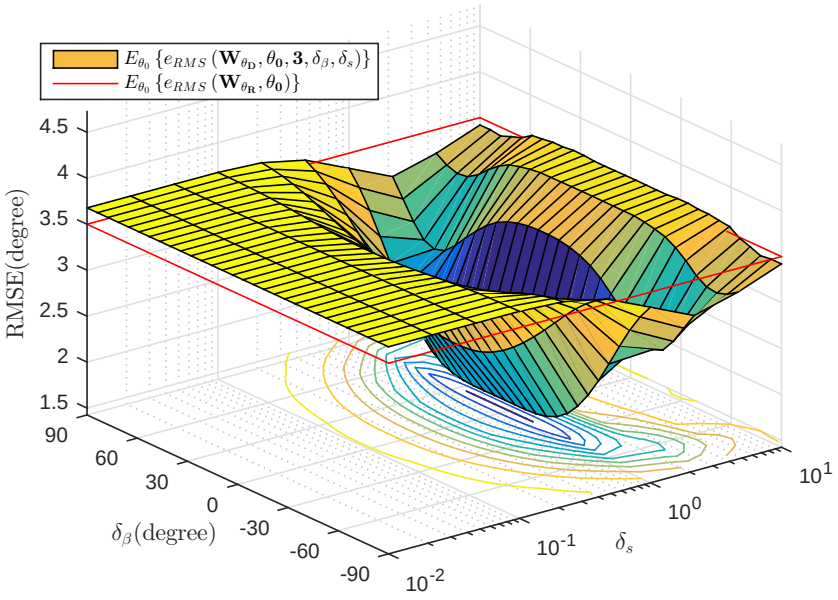

Figure 5.9: The averaged RMSE over parameter space of the proposed measurement matrices in the chase of unknown complex magnitude and phase for $\mathbf{3}^o$ perturbation level ($\boldsymbol{\delta_\theta} = \mathbf{3}^o$).

histogram of the difference in the magnitude and the phase concentrate as SNR level increases. Therefore, the unknown components of the complex amplitude, δ_s and δ_β, are estimated with lower error. As it will be pointed out just below, the lower level of $|s| - |\widehat{s}|$ and $\angle(s) - \angle(\widehat{s})$, allows the proposed technique to yield higher estimation performance for the estimation of DoA. Thus, higher levels of SNR do not only improve the estimation over the c_0 term defined in (A.8) but also decreasing the estimation error in the complex amplitude as in (5.9).

In Fig. 5.13, the averaged RMSE of the proposed measurement matrices designed on $\widehat{\boldsymbol{\theta}}$ that is obtained by *SSIC* with various numbers of sectors at different levels of SNR. In this case, the perturbation vector in the design corresponds to $\boldsymbol{\delta_\theta} = \boldsymbol{\theta}_0 - \widehat{\boldsymbol{\theta}}$, the unknown phase in the complex amplitude is $\delta_\beta = \angle(s) - \angle(\widehat{s})$ and the unknown component of the magnitude of the complex amplitude is $\delta_s = \frac{|s-\widehat{s}|}{s_0}$. Therefore, $\mathrm{E}_{\boldsymbol{\theta}_0}\left\{\mathrm{e}_{RMS}\left(\boldsymbol{W}_{\widehat{\boldsymbol{\theta}}}, \boldsymbol{\theta}_0, \boldsymbol{\theta}_0 - \widehat{\boldsymbol{\theta}}, \angle(s) - \angle(\widehat{s}), \frac{|s-\widehat{s}|}{s_0}\right)\right\}$ is indicated for various number of sectors and for Gaussian random matrices in Fig. 5.13. For comparison, the CRLB under no perturbation and known complex amplitude of

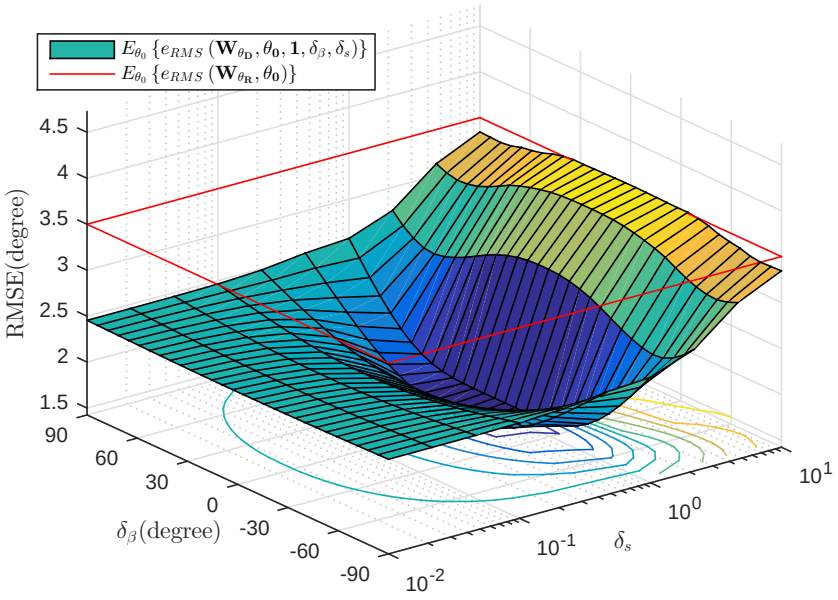

Figure 5.10: The averaged RMSE over parameter space of the proposed measurement matrices in the chase of unknown complex magnitude and phase for $\mathbf{1}^o$ perturbation level ($\boldsymbol{\delta_\theta} = \mathbf{1}^o$).

the proposed measurement matrices is also presented. It is observed that when *SSIC* algorithm is utilized with $N_S \geq 3$, the proposed measurement matrices yield improved estimation performance for the range of practical SNR levels. When $N_S = 2$ and $N_S = 1$, the proposed measurement matrices are favorable after SNR levels of $1.2dB$ and $2.5dB$, respectively. The reasons behind such an observation can be explained as follows. Under low SNR and $N_S < 3$, the *SSIC* is tend to provide higher RMSE compared to Gaussian matrices as illustrated in Fig. 5.16. Thus, the performance of the proposed measurement matrices degrades below the level of Gaussian matrices with the respectively higher levels of $\boldsymbol{\delta_\theta}$, δ_β and δ_s. As SNR increases, the performance of the proposed measurement matrices enhances with the lower levels of $\boldsymbol{\delta_\theta}$, δ_β. For $N_S \geq 3$, *SSIC* algorithm estimates $\boldsymbol{\theta}_0$ and s with sufficiently low levels of $\boldsymbol{\delta_\theta}$, δ_β leading the proposed technique outperforms Gaussian matrices.

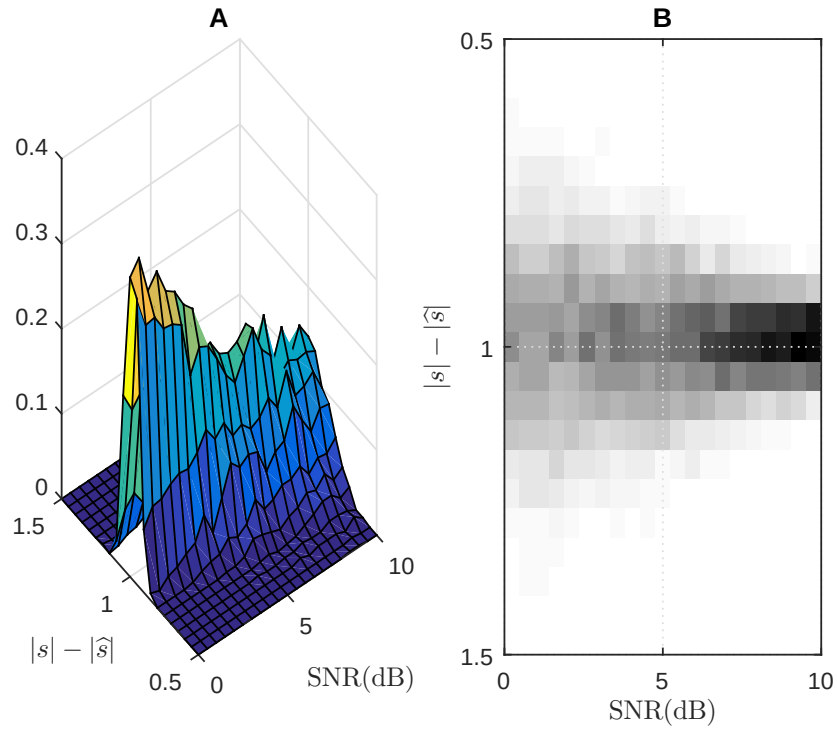

Figure 5.11: The histogram of the averaged $|s| - |\widehat{s}|$ computed over the parameter space as a function of SNR, when *SSIC* is used with 6 number of sectors.

5.3 Performance of the Proposed Measurement Matrix Design Algorithm for Surveillance and Tracking

In this section, the surveillance and tracking performance of the proposed techniques are assessed and compared with Gaussian matrices. The performance of the proposed partitioning is discussed in Section 5.3.1. The ROC analysis of *SSIC* algorithm is performed and compared with Gaussian matrices in Section 5.3.2. Furthermore, in Section 5.4, the performance of the proposed adaptive tracking algorithm is demonstrated. In Section 5.5, the performance of the proposed measurement matrices under the presence of multiple targets is investigated.

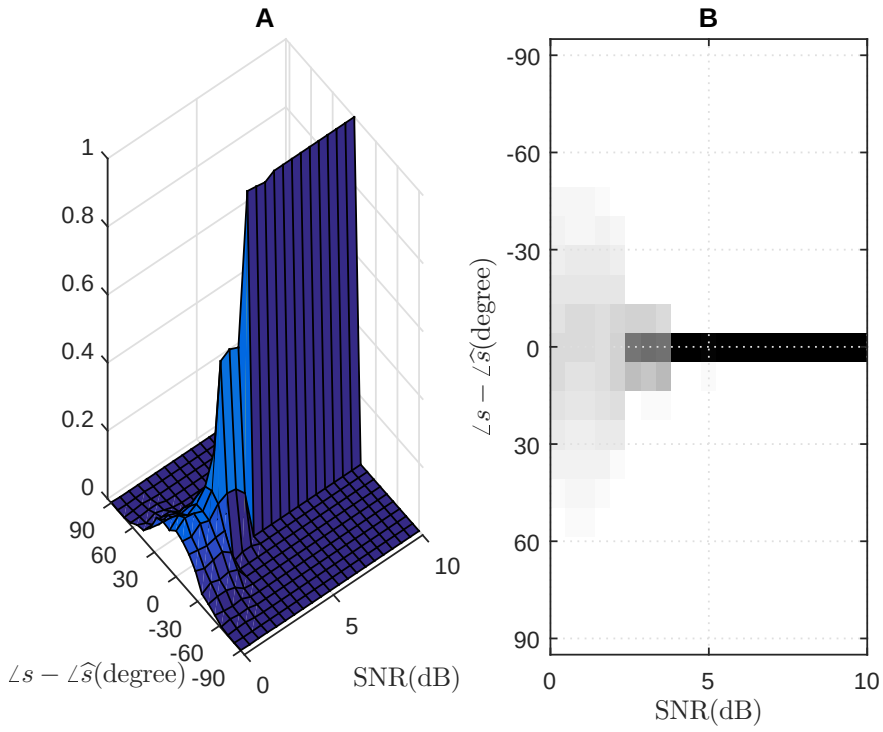

Figure 5.12: The histogram of the averaged $\angle(s) - \angle(\widehat{s})$ computed over the parameter space as a function of SNR, when *SSIC* is used with 6 number of sectors.

5.3.1 Performance of the Proposed Partitioning Technique

Suppose that $\breve{\boldsymbol{\theta}}_g$ is a point in the surveillance scene, which lies on sector $\mathcal{S}_p$, i.e., $\breve{\boldsymbol{\theta}}_g \in \mathcal{S}_p$. The surveillance of sector $\breve{\boldsymbol{\theta}}_g$ is conducted based on measurement matrix $\boldsymbol{W}_{\widetilde{\boldsymbol{\theta}}_p}$. Therefore, $\text{Tr}\left\{\boldsymbol{J}^{-1}\left(\boldsymbol{W}_{\widetilde{\boldsymbol{\theta}}_p} \mid I_g = p, \breve{\boldsymbol{\theta}}_g\right)\right\}$ is related to the surveillance performance of a target with DoA $\breve{\boldsymbol{\theta}}_g$ when it is monitored by measurement matrix $\boldsymbol{W}_{\widetilde{\boldsymbol{\theta}}_p}$.

To investigate the performance of the proposed surveillance approach in an effective manner, a metric measuring the optimality of the proposed partitioning

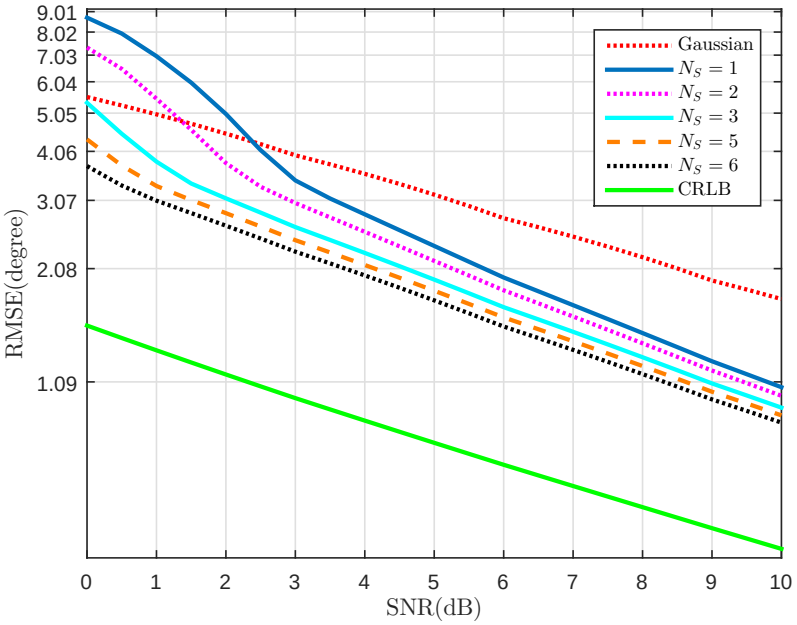

Figure 5.13: The averaged RMSE of the proposed measurement matrices when the design vector and the complex amplitude are estimated by *SSIC* with various numbers of sectors at different levels of SNR.

technique is defined as follows:

$$\mathrm{O}\left\{\breve{\boldsymbol{\theta}}_g\right\} = \frac{\mathrm{Tr}\left\{\boldsymbol{J}^{-1}\left(\boldsymbol{W}_{\breve{\boldsymbol{\theta}}_g}, \breve{\boldsymbol{\theta}}_g\right)\right\}}{\mathrm{Tr}\left\{\boldsymbol{J}^{-1}\left(\boldsymbol{W}_{\tilde{\boldsymbol{\theta}}_b} \mid I_g = b, \breve{\boldsymbol{\theta}}_g\right)\right\}} \tag{5.10}$$

where $\mathrm{Tr}\left\{\boldsymbol{J}^{-1}\left(\boldsymbol{W}_{\breve{\boldsymbol{\theta}}_g}, \breve{\boldsymbol{\theta}}_g\right)\right\}$ refers to the case when a target with DoA $\breve{\boldsymbol{\theta}}_g$ is detected with the measurement matrix $\boldsymbol{W}_{\breve{\boldsymbol{\theta}}_g}$, i.e., the optimal case. It can be shown that $0 \leq \mathrm{O}\left\{\breve{\boldsymbol{\theta}}_g\right\} \leq 1$. Small values of $\mathrm{O}\left\{\breve{\boldsymbol{\theta}}_g\right\}$ correspond to low detection probability whereas large values of $\mathrm{O}\left\{\breve{\boldsymbol{\theta}}_g\right\}$ are associated with high probability of detection. When $\mathrm{O}\left\{\breve{\boldsymbol{\theta}}_g\right\} = 1$, the proposed surveillance algorithm yields the best possible performance.

In Fig. 5.14, $\mathrm{O}\left\{\breve{\boldsymbol{\theta}}_g\right\}$ is illustrated for a setup with $N_S = 6$ sectors, where $N = 24$ sensors are compressed to $M = 2$ measurements for each sector; hence 12 in total. The corresponding partioning of the parameter space is given in Fig. 5.15, where each sector is shown by a different color. In Fig. 5.14, it can be

observed that $\mathrm{O}\left\{\breve{\boldsymbol{\theta}}_g\right\}$ is close to 1 around the 6 points where the measurement matrices are designed for each sector, $\left\{\widetilde{\boldsymbol{\theta}}_1, ..., \widetilde{\boldsymbol{\theta}}_6\right\}$, as expected. Roughly speaking, in the vicinity of the design points, i.e., $\left\|\widetilde{\boldsymbol{\theta}}_b - \breve{\boldsymbol{\theta}}_g\right\| < \epsilon\left(\widetilde{\boldsymbol{\theta}}_b\right)$, where $\widetilde{\boldsymbol{\theta}}_b$ is the corresponding design point of $\widetilde{\boldsymbol{\theta}}_b$ and $\epsilon\left(\widetilde{\boldsymbol{\theta}}_b\right)$ is a constant depending on $\widetilde{\boldsymbol{\theta}}_b$, it is observed that $\mathrm{O}\left\{\breve{\boldsymbol{\theta}}_g\right\}$ gets smaller as $\breve{\boldsymbol{\theta}}_g$ gets away from $\breve{\boldsymbol{\theta}}_b$. In other words, in the vicinity of the design points, $\mathrm{O}\left\{\breve{\boldsymbol{\theta}}_g\right\}$ is inversely proportional to the distance from the design point. For the distant points from the design points, on the other hand, $\mathrm{O}\left\{\breve{\boldsymbol{\theta}}_g\right\}$ is non-convex. As it is shown in Fig. 5.15, the proposed partitioning technique yields non-convex sectors on the surveillance space.

In Fig. 5.16, the averaged CRLB over the parameter space is presented as a function of N_S $\left(\mathrm{E}_{\breve{\boldsymbol{\theta}}_g}\left\{\mathrm{e}_{RMS}\left(\boldsymbol{W}_{\boldsymbol{\theta}_b|I_g=b}, \breve{\boldsymbol{\theta}}_g\right)\right\}\right)$. The averaged CRLB for the optimal case, where each point on the surveillance space is monitored by the measurement matrix designed on the same point, and for the random matrices are also shown in Fig. 5.16. It is observed that after $N_S = 3$ sectors, the proposed measurement design matrices designed on the points computed by the proposed portioning technique enhances the performance over the widely used random matrices.

5.3.2 Receiver Operating Characteristics (ROC) Analysis

In *SSIC* algorithm, the proposed measurement matrices are used with $M = 2$ for N_S sectors; hence $2N_S$ measurements exists in total. For a fair comparison of *SSIC* algorithm with the random Gaussian measurement matrices, a single measurement matrix with $M = 2N_S$ measurements is generated.

To perform surveillance, a very similar approach to *SSIC* is followed except that only one likelihood is computed using a single measurement matrix instead of N_S likelihoods in the case of *SSIC* algorithm. In Fig. 5.17 and Fig. 5.18, the Receiver Operating Characteristics (ROC) curves are shown for both *SSIC* algorithm and a similar surveillance technique using random matrices with $N_S =$

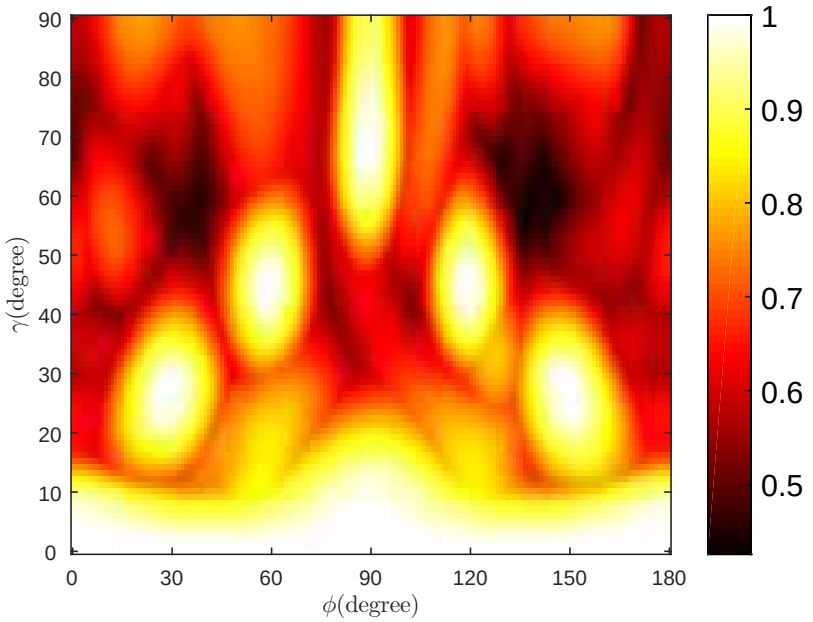

Figure 5.14: A normalized CRLB $\left(\mathrm{O}\left\{\breve{\boldsymbol{\theta}}_g\right\}\right)$ of the partitioned parameter space as a function of elevation (γ) and azimuth (ϕ) when 6 sectors are used by the proposed partitioning technique.

3 and $N_S = 6$ at the SNRs of 0dB and 3dB, respectively. It is observed that *SSIC* provides improvements in detection performance especially at low SNRs. As indicated in Fig. 5.17, *SSIC* with 6 measurements in total yields more accurate detection results than using the random matrices with $M = 12$ (or $M = 6$).

5.4 Performance of Adaptive Target Tracking via Proposed Measurement Matrix Design

To measure the adaptive target tracking performance of the proposed measurement design algorithm described in Section 3.2, it is assumed that the initial position of a target ($\boldsymbol{\theta}^1$) is unknown at the first snapshot and it moves under a constant velocity model. To estimate the DoA of a target at the i^{th} snapshot, the measurements are captured through $\boldsymbol{W}_{\widehat{\boldsymbol{\theta}}^{i|i-1}}$ and $\boldsymbol{W}_R$, where $\boldsymbol{W}_{\widehat{\boldsymbol{\theta}}^{i|i-1}}$ is the updated version of the previous DoA estimation via the underlying constant

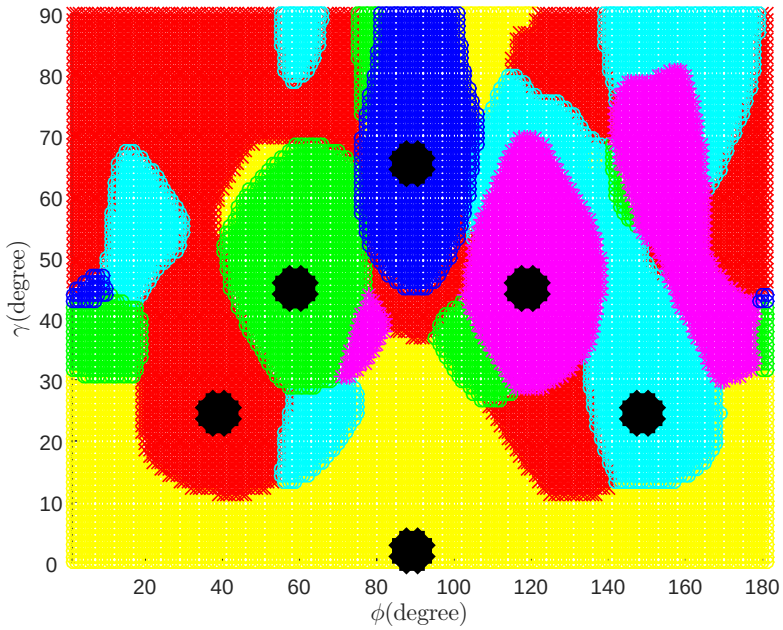

Figure 5.15: The corresponding sectors given Fig. 5.14, where each of them is depicted with a different color.

velocity model. For an SNR of 3dB, the averaged RMSEs for DoA estimation over the parameter space as a function of the snapshot number are illustrated as $\mathrm{E}_{\boldsymbol{\theta}_0}\left\{\mathrm{e}_{RMS}\left(\boldsymbol{W}_R, \boldsymbol{\theta}\right)\right\}$ and $\mathrm{E}_{\boldsymbol{\theta}_0}\left\{\mathrm{e}_{RMS}\left(\boldsymbol{W}_{\widehat{\boldsymbol{\theta}}^{i|i-1}}, \boldsymbol{\theta}\right)\right\}$ in Fig. 5.19 for the proposed measurement design technique and the random matrices, respectively. At the first couple of snapshots (e.g., $i \leq 3$), $\boldsymbol{W}_R$ provides slightly better performance due to the distance between $\boldsymbol{\theta}_0$ and $\widehat{\boldsymbol{\theta}_0}$. As the difference between the estimated DoA and the actual DoA at the previous snapshot decreases, the proposed adaptive measurement design technique yields superior performance compared to random matrices.

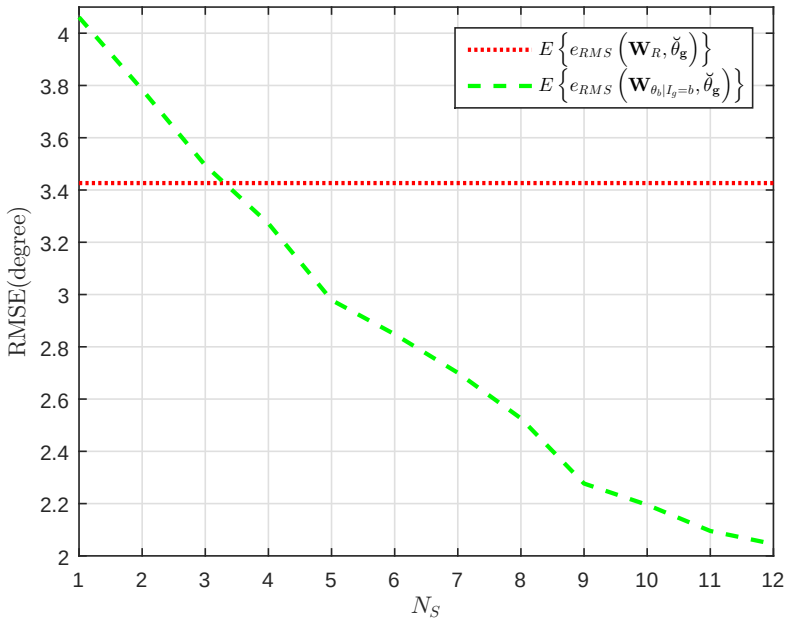

Figure 5.16: The averaged CRLB over the parameter space as a function of the number of sectors (N_S) $\left(\mathrm{E}_{\breve{\boldsymbol{\theta}}_g}\left\{\mathrm{e}_{RMS}\left(\boldsymbol{W}_{\boldsymbol{\theta}_b|I_g=b}, \breve{\boldsymbol{\theta}}_g\right)\right\}\right)$ (green) and the averaged CRLB for the random matrices (red).

5.5 Performance of the Proposed Multi-Target Tracking Technique

In this section, the performance degradation of the proposed design technique is analyzed for the multi-target case. Suppose that two targets are currently tracked in the scene with the input signal at the sensor array being given by

$$\boldsymbol{x}\left(\boldsymbol{\theta}_1, \boldsymbol{\theta}_2, s_1, s_2, \boldsymbol{t}\right) = s_1 e^{j\omega(\boldsymbol{t}+\boldsymbol{\tau}(\boldsymbol{\theta}_1))} + s_2 e^{j\omega(\boldsymbol{t}+\boldsymbol{\tau}(\boldsymbol{\theta}_2))}, \tag{5.11}$$

where $\boldsymbol{\theta}_2 = \boldsymbol{\theta}_{2_D} + \boldsymbol{\delta}_I$; $\boldsymbol{\theta}_{2_D}$ is the known design point for the second currently tracked target and $\boldsymbol{\delta}_I \sim \mathcal{N}\left(\mathbf{0}, \sigma_I^2 \boldsymbol{I}\right)$. Under this signal model, the DoA of the first target is estimated by via the $ATSIC$algorithm, i.e., by canceling the impact from second target via its estimated position $\widehat{\boldsymbol{\theta}}_2$.

In Fig. 5.20, $\mathrm{E}_{\boldsymbol{\theta}_0}\left\{\mathrm{e}_{RMS}\left(\boldsymbol{W}_{\boldsymbol{\theta}_1}, \boldsymbol{\theta}_1\right)\right\}$ is demonstrated as a function the signal-to-interference ratio defined as $\frac{|s_1|^2}{|s_2|^2}$ for three different levels of σ_I; $\sigma_I = 5^0$, $\sigma_I = 1^0$

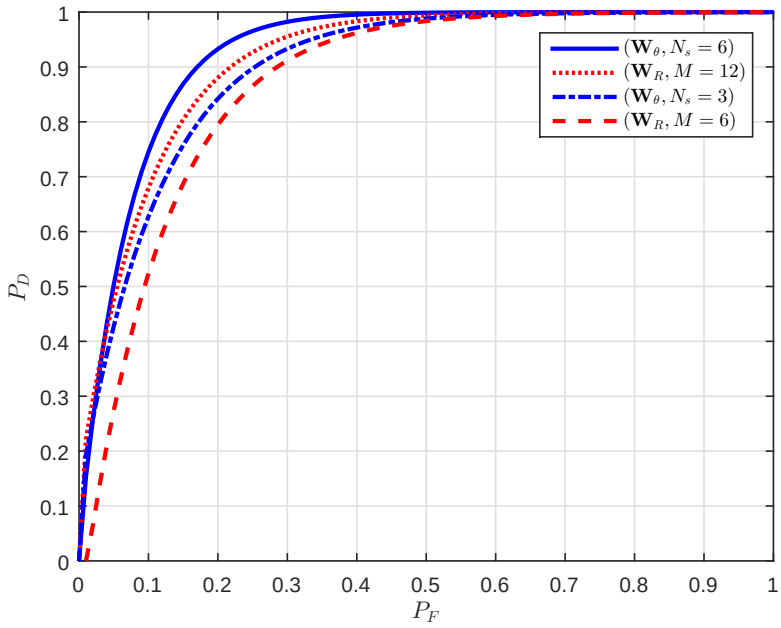

Figure 5.17: The ROC of the proposed technique with 6 and 3 sectors (blue), the ROC of the proposed technique with Gaussian matrices using 6 and 12 sonsr outputs (blue) under $0dB$ SNR.

and no interference ($\sigma_I = 0^0$). It is observed that although interference deteriorates the performance of the proposed measurement design to adaptively track a target, it still provides more accurate results compared to the results for the random matrices approach which are in fact obtained *in the absence of interference.*

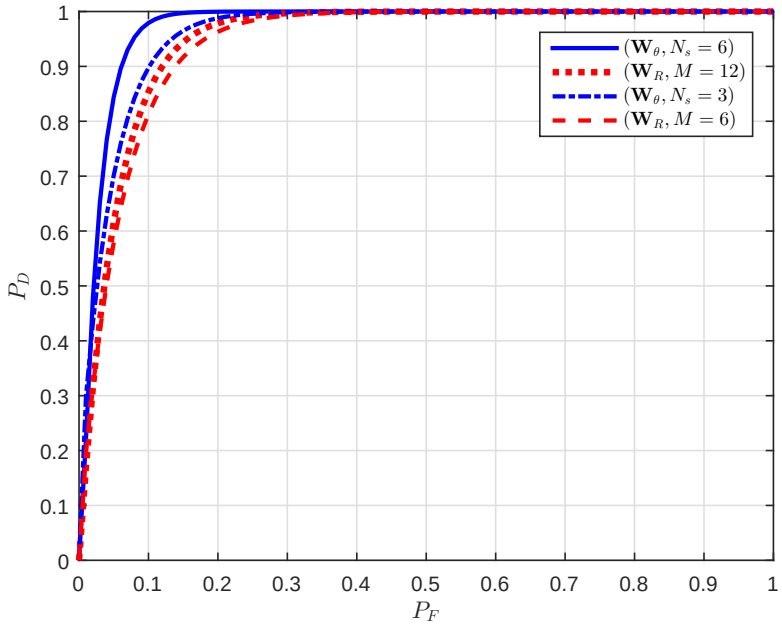

Figure 5.18: The ROC of the proposed technique with 6 and 3 sectors (blue), the ROC of the proposed technique with Gaussian matrices using 6 and 12 sonsr outputs (blue) under $3dB$ SNR.

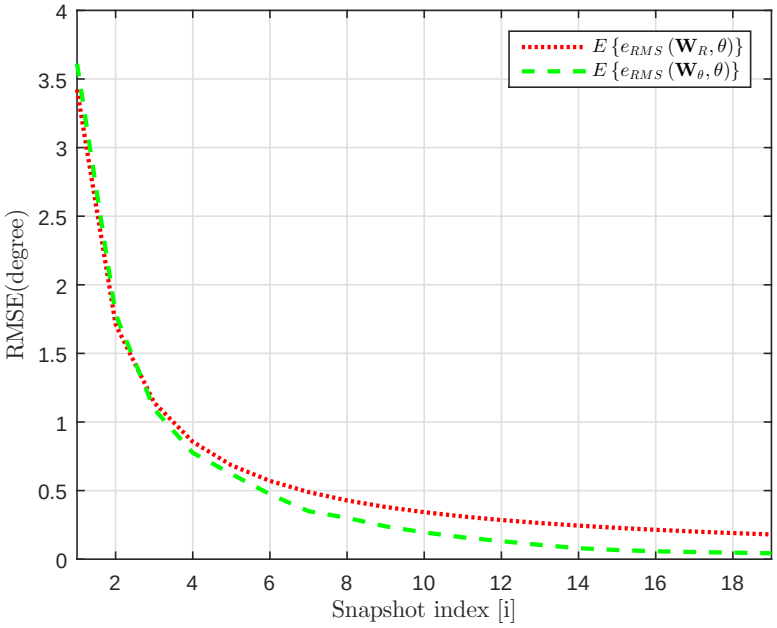

Figure 5.19: The averaged RMSE over parameter space for the adaptive measurement algorithm (green) and Gaussian random matrices (red) as a function of snapshot index.

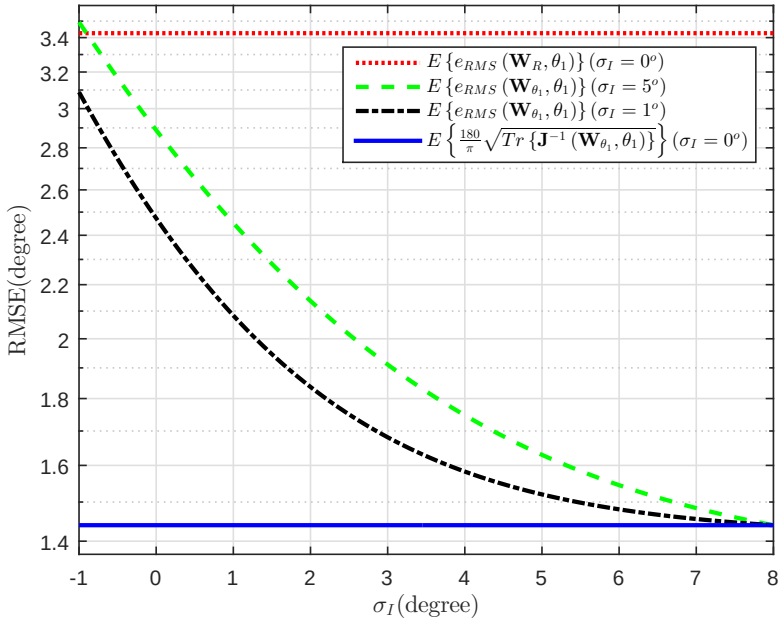

Figure 5.20: The averaged RMSE as a function of SIR for for $\sigma_I = 5^o$ (green) and $\sigma_I = 1^o$ (black), the averaged CRLB for no interference (blue) and the averaged RMSE when random matrices are used under no interference (red).

Chapter 6

Conclusions

In this thesis, DoA estimation problems are investigated within CS framework. A novel anolog combiner scheme, unlike traditional methods in the literature, is employed to compress the sensor outputs before analog-to-digital conversion. Analog combiners are formulated as measurement matrices in the signal model.

Measurement matrices are designed in order to minimize the CRLB of a single target, which provides a lower bound for the estimation of DoA. The minimization problem of the CRLB is considered under the constraint, that imposes the gram matrix of the measurement to be identity matrix, in order to avoid redundant measurements and coloring the noise. The CRLB is first derived as a function of DoA, measurement matrix and the complex amplitude of the input signal. It is shown that the minimization of the CRLB tackles significant challenges in analytical domain when the complex amplitude is taken as a nuisance parameter in the Fisher Information matrix. Hence, a practical approach is followed, where the complex amplitude is assumed to be known before the design of measurement matrices. In this case, a fast closed form solution to the minimization problem is proposed and it is proved that the proposed measurement matrices minimize the CRLB for symmetric array alignments. It is also shown that it is sufficient to minimize the CRLB using the measurement matrices consisting of 2 orthonormal rows in total, that are allocated for elevation and azimuth.

Novel surveillance (detection) and tracking (estimation) techniques that are built upon the proposed measurement matrices are developed. Surveillance, aiming to detect newly emerging targets in the scene, is performed by following a sequential approach. The parameter space is split to MECE regions, as referred to as sectors, so that the surveillance of each sector is conducted individually in the consecutive snapshots. A GLRT-like algorithm called Sequential Surveillance with Interference Cancellation (*SSIC*) algorithm is proposed. *SSIC* algorithm first cancels the interference from the previous detected targets. Then, for each sector, the likelihood ratio is computed by using the estimated parameters over the measurements that are captured via a carefully designed measurement matrix. To design the set of sectors and the corresponding design vectors, a minmax type optimization problem is formulated to ensure robust surveillance performance. The sectors and the design vectors are formed so that the worst case performance (maximum error) in the sectors are minimized. Since it is very challenging to obtain a closed form solution for the formulated optimization problem, a greedy type algorithm is developed. In the first step of the proposed partitioning algorithm, the training set is generated by fine quantizatizing of the parameter space and the initial design vectors are randomly designated. Then, using an iterative approach, each vector in the training set is assigned to a design vector which yields the minimum CRLB. Therefore, the set of possibly (non-convex) sectors are formed. Afterwards, for each sector, the design vector of a sector is updated so that the maximum CRLB within the sector is minimized. The convergence of the algorithm is detected when the sectors and their corresponding design vectors remained unchanged in successive iterations. Moreover, an adaptive target tracking technique is introduced. For each snapshot, measurement matrices are designed on the vector that is acquired by iteratively updating the estimated DoA of the previous snapshot by a properly chosen state dynamics model.

The surveillance and tracking techniques developed for a single target are also extended to the case of multiple targets in the scene. A novel tracking algorithm, as referred to as Adaptive Tracking of Multiple Targets using Successive Interference Cancellation (*ATSIC*), is proposed. *ATSIC* algorithm utilizes for each target an adaptive measurement matrix that is designed on the predicted DoA

of the corresponding target. *ATSIC* also cancels the interference employing a SIC-type technique. An algorithm that combines *SSIC* and *ATSIC* to jointly perform the surveillance and tracking in the scene is also introduced.

The performance of the surveillance and tracking techniques using the proposed and Gaussian matrices are comprehensively evaluated and compared via a set of simulations. It is shown that the proposed measurement matrix yields 0.43 of the RMSE achieved by Gaussian matrices, on average. It provides significant improvements especially for small and high elevation angles. It is possible to obtain the same RMSE level achieved by Gaussian matrices under 15dB less SNR when proposed matrices are utilized. In addition, it is demonstrated that the proposed measurement matrices are robust against the perturbation in the design vector from the actual DoA. The proposed matrices enhances estimation performance if he perturbation in elevation and azimuth is less than 5.7^o, which is achieved by the proposed techniques at the most of feasible SNR ranges. The impact of unknown complex amplitude is also investigated. It is illustrated that if the perturbation in the design vector is less than 3^o, the proposed technique outperform Gaussian matrices independently of any level of uncertainty in the complex amplitude. For higher level of perturbation, it still tend to provide performance improvements over Gaussian matrices depending on the unknown phase of the complex amplitude. Most importantly, it is demonstrated that using the proposed measurement matrices leads significant performance enhancement over Gaussian matrices in real-case scenario, where the initial DoA and the complex amplitude are first estimated by *SSIC* and the measurement matrices are designed on initial DoA estimation. When more than 2 sectors are used in *SSIC*, the performance of Gaussian matrices are exceeded at all SNR levels. For less than 3 sectors, the performance of Gaussian matrices are still exceeded at all SNR levels grater than 1.5dB. Furthermore, it is shown that the proposed measurement matrices provide better ROC curves in the sense that it provides higher true detection probabilities for most of false positive levels.

Bibliography

[1] T. E. Tuncer and B. Friedlander, *Classical and modern direction-of-arrival estimation*. Academic Press, 2009.

[2] L. C. Godara, "Application of antenna arrays to mobile communications. ii. beam-forming and direction-of-arrival considerations," *Proceedings of the IEEE*, vol. 85, no. 8, pp. 1195–1245, 1997.

[3] Z. Wang, J. Xie, G. Zhou, Z. Ji, and T. Quan, "Real-valued sparse representation for single snapshot direction-of-arrival estimation in shipborne high-frequency surface wave radar," *IET Radar, Sonar & Navigation*, vol. 9, no. 9, pp. 1314–1322, 2015.

[4] R. Rajagopal and P. Rao, "Generalised algorithm for doa estimation in a passive sonar," in *IEE Proceedings F-Radar and Signal Processing*, vol. 140, pp. 12–20, IET, 1993.

[5] H. Amiri, H. Amindavar, and M. Kamarei, "Underwater noise modeling and direction-finding based on conditional heteroscedastic time series," in *2006 IEEE International Conference on Acoustics Speech and Signal Processing Proceedings*, vol. 4, pp. IV–IV, IEEE, 2006.

[6] M. Baum and P. Willett, "Mmospa-based direction-of-arrival tracking with a passive sonar arrayan experimental study," in *Information Fusion (Fusion), 2015 18th International Conference on*, pp. 1382–1387, IEEE, 2015.

[7] T. W. Pirinen, J. Yli-Hietanen, P. Pertila, and A. Visa, "Detection and compensation of sensor malfunction in time delay based direction of arrival

estimation," in *Circuits and Systems, 2004. ISCAS'04. Proceedings of the 2004 International Symposium on*, vol. 4, pp. IV–872, IEEE, 2004.

[8] A. K. Khan, T. Onoue, K. Hashiodani, Y. Fukumizu, and H. Yamauchi, "Signal and noise separation in medical diagnostic system based on independent component analysis," in *Circuits and Systems (APCCAS), 2010 IEEE Asia Pacific Conference on*, pp. 812–815, IEEE, 2010.

[9] A. Rabinovich, A. Feuer, and Z. Friedman, "Multi-line transmission combined with minimum variance beamforming in medical ultrasound imaging," *IEEE transactions on ultrasonics, ferroelectrics, and frequency control*, vol. 62, no. 5, pp. 814–827, 2015.

[10] T. S. Rappaport, J. H. Reed, and B. D. Woerner, "Position location using wireless communications on highways of the future," *IEEE communications Magazine*, vol. 34, no. 10, pp. 33–41, 1996.

[11] A. J. Paulraj and C. B. Papadias, "Space-time processing for wireless communications," *IEEE Signal Processing Magazine*, vol. 14, no. 6, pp. 49–83, 1997.

[12] E. Greenberg and M. Naor, "Direction of arrival estimation in urban multipath environments," in *2016 10th European Conference on Antennas and Propagation (EuCAP)*, pp. 1–5, IEEE, 2016.

[13] K. G. Jansky, "Directional studies of atmospherics at high frequencies," in *Classics in Radio Astronomy*, pp. 10–22, Springer, 1932.

[14] M. I. Miller and D. R. Fuhrmann, "Maximum-likelihood narrow-band direction finding and the em algorithm," *IEEE Transactions on Acoustics, Speech, and Signal Processing*, vol. 38, no. 9, pp. 1560–1577, 1990.

[15] T.-J. Shan, M. Wax, and T. Kailath, "On spatial smoothing for direction-of-arrival estimation of coherent signals," *IEEE Trans. Acoust. Speech Signal Process*, vol. 33, no. 4, pp. 806–811, 1985.

[16] M. Hawkes and A. Nehorai, "Acoustic vector-sensor beamforming and capon direction estimation," *IEEE Transactions on Signal Processing*, vol. 46, no. 9, pp. 2291–2304, 1998.

[17] Z. Yang, L. Xie, and C. Zhang, "Off-grid direction of arrival estimation using sparse bayesian inference," *IEEE Transactions on Signal Processing*, vol. 61, no. 1, pp. 38–43, 2013.

[18] R. Schmidt, "Multiple emitter location and signal parameter estimation," *IEEE transactions on antennas and propagation*, vol. 34, no. 3, pp. 276–280, 1986.

[19] R. Roy and T. Kailath, "Esprit-estimation of signal parameters via rotational invariance techniques," *IEEE Transactions on Acoustics, Speech, and Signal Processing*, vol. 37, no. 7, pp. 984–995, 1989.

[20] E. J. Candès, J. Romberg, and T. Tao, "Robust uncertainty principles: Exact signal reconstruction from highly incomplete frequency information," *IEEE Transactions on Information Theory*, vol. 52, no. 2, pp. 489–509, 2006.

[21] D. L. Donoho and X. Huo, "Uncertainty principles and ideal atomic decomposition," *IEEE Transactions on Information Theory*, vol. 47, no. 7, pp. 2845–2862, 2001.

[22] J. Haupt and R. Nowak, "Signal reconstruction from noisy random projections," *Information Theory, IEEE Transactions on*, vol. 52, no. 9, pp. 4036–4048, 2006.

[23] R. G. Baraniuk, "Compressive sensing," *IEEE Signal Processing Magazine*, vol. 24, no. 4, 2007.

[24] J. H. Ender, "On compressive sensing applied to radar," *Signal Processing*, vol. 90, no. 5, pp. 1402–1414, 2010.

[25] A. Gurbuz, J. McClellan, and V. Cevher, "A compressive beamforming method," in *IEEE International Conference on Acoustics, Speech and Signal Processing*, pp. 2617–2620, March 2008.

[26] Z.-M. Liu, Z.-T. Huang, and Y.-Y. Zhou, "An efficient maximum likelihood method for direction-of-arrival estimation via sparse bayesian learning," *IEEE Transactions on Wireless Communications*, vol. 11, no. 10, pp. 1–11, 2012.

[27] O. Teke, A. C. Gurbuz, and O. Arikan, "A robust compressive sensing based technique for reconstruction of sparse radar scenes," *Digital Signal Processing*, vol. 27, pp. 23–32, 2014.

[28] F. Roemer, M. Ibrahim, R. Alieiev, M. Landmann, R. S. Thomae, and G. D. Galdo, "Polarimetric compressive sensing based doa estimation," in *18th International ITG Workshop on Smart Antennas (WSA)*, pp. 1–8, VDE, 2014.

[29] Y. Yu, A. P. Petropulu, and H. V. Poor, "Compressive sensing for mimo radar," in *Acoustics, Speech and Signal Processing, 2009. ICASSP 2009. IEEE International Conference on*, pp. 3017–3020, IEEE, 2009.

[30] J. M. Kim, O. K. Lee, and J. C. Ye, "Compressive music: revisiting the link between compressive sensing and array signal processing," *Information Theory, IEEE Transactions on*, vol. 58, no. 1, pp. 278–301, 2012.

[31] I. Bilik, "Spatial compressive sensing for direction-of-arrival estimation of multiple sources using dynamic sensor arrays," *Aerospace and Electronic Systems, IEEE Transactions on*, vol. 47, no. 3, pp. 1754–1769, 2011.

[32] D. H. Johnson and D. E. Dudgeon, *Array signal processing: concepts and techniques*. Simon & Schuster, 1992.

[33] S. G. Mallat and Z. Zhang, "Matching pursuits with time-frequency dictionaries," *Signal Processing, IEEE Transactions on*, vol. 41, no. 12, pp. 3397–3415, 1993.

[34] J. Tropp, A. C. Gilbert, *et al.*, "Signal recovery from random measurements via orthogonal matching pursuit," *Information Theory, IEEE Transactions on*, vol. 53, no. 12, pp. 4655–4666, 2007.

[35] T. Blumensath and M. E. Davies, "Iterative hard thresholding for compressed sensing," *Applied and Computational Harmonic Analysis*, vol. 27, no. 3, pp. 265–274, 2009.

[36] G. Tang, B. N. Bhaskar, P. Shah, and B. Recht, "Compressed sensing off the grid," *Information Theory, IEEE Transactions on*, vol. 59, no. 11, pp. 7465–7490, 2013.

[37] W. Si, X. Qu, Z. Qu, and P. Zhao, "Off-grid doa estimation via real-valued sparse bayesian method in compressed sensing," *Circuits, Systems, and Signal Processing*, pp. 1–17, 2016.

[38] M. Elad, "Optimized projections for compressed sensing," *IEEE Transactions on Signal Processing*, vol. 55, pp. 5695–5702, Dec, 2007.

[39] L. Zelnik-Manor, K. Rosenblum, and Y. C. Eldar, "Sensing matrix optimization for block-sparse decoding," *IEEE Transactions on Signal Processing*, vol. 59, no. 9, pp. 4300–4312, 2011.

[40] J. M. Duarte-Carvajalino and G. Sapiro, "Learning to sense sparse signals: Simultaneous sensing matrix and sparsifying dictionary optimization," *IEEE Transactions on Image Processing*, vol. 18, no. 7, pp. 1395–1408, 2009.

[41] Y. Yu, A. P. Petropulu, and H. V. Poor, "Measurement matrix design for compressive sensing–based MIMO radar," *IEEE Transactions on Signal Processing*, vol. 59, no. 11, pp. 5338–5352, 2011.

[42] P. Chen and L. Wu, "Joint design transmission waveform and sensing matrix for the compressive sensing radar," in *Communication Systems, Networks & Digital Signal Processing (CSNDSP), 2014 9th International Symposium on*, pp. 558–563, IEEE, 2014.

[43] J. Zhang, D. Zhu, and G. Zhang, "Adaptive compressed sensing radar oriented toward cognitive detection in dynamic sparse target scene," *IEEE Transactions on Signal Processing*, vol. 60, no. 4, pp. 1718–1729, 2012.

[44] J. M. Duarte-Carvajalino, G. Yu, L. Carin, and G. Sapiro, "Task-driven adaptive statistical compressive sensing of Gaussian mixture models," *IEEE Transactions on Signal Processing*, vol. 61, no. 3, pp. 585–600, 2013.

[45] J. Mairal, F. Bach, and J. Ponce, "Task-driven dictionary learning," *IEEE Transactions on Pattern Analysis and Machine Intelligence*, vol. 34, pp. 791–804, April 2012.

[46] M. Sharp, M. Pekala, J. Nanzer, I.-J. Wang, D. Lucarelli, and K. Lauritzen, "Exploiting adaptive beamforming for compressive measurements," in *Sensor Array and Multichannel Signal Processing Workshop (SAM), 2012 IEEE 7th*, pp. 337–340, IEEE, 2012.

[47] M. Ibrahim, F. Roemer, and G. Del Galdo, "On the design of the measurement matrix for compressed sensing based doa estimation," in *Acoustics, Speech and Signal Processing (ICASSP), 2015 IEEE International Conference on*, pp. 3631–3635, IEEE, 2015.

[48] M. Gromann, V. Ramirreddy, J. Knig, M. Landmann, F. Rmer, G. D. Galdo, and R. Perthold, "Antenna array optimization strategies for robust direction finding," in *Proc. 10th Europ. Conf. on Antennas and Propagation (EuCAP 2016)*, (Davos, Switzerland), Apr. 2016.

[49] D. R. Fuhrmann, "Adaptive sensing of target signature with unknown amplitude," in *Signals, Systems and Computers, 2008 42nd Asilomar Conference on*, pp. 218–222, IEEE, 2008.

[50] A. Poudel and D. R. Fuhrmann, "Adaptive sensing and target tracking of a simple point target with online measurement selection," in *Conference Record of the Forty Fourth Asilomar Conference on Signals, Systems and Computers (ASILOMAR)*, pp. 2017–2020, 2010.

[51] J. P. Helferty and D. R. Mudgett, "Optimal observer trajectories for bearings only tracking by minimizing the trace of the cramer-rao lower bound," in *Proceedings of the 32nd IEEE Conference on Decision and Control,*, pp. 936–939, 1993.

[52] B. Yang and J. Scheuing, "Cramer-rao bound and optimum sensor array for source localization from time differences of arrival," in *Acoustics, Speech, and Signal Processing, 2005. Proceedings. (ICASSP '05). IEEE International Conference on*, vol. 4, pp. 961–964., March 2005.

[53] M. Carlin, P. Rocca, G. Oliveri, F. Viani, and A. Massa, "Directions-of-arrival estimation through bayesian compressive sensing strategies," *Antennas and Propagation, IEEE Transactions on*, vol. 61, no. 7, pp. 3828–3838, 2013.

[54] Y. Wang, G. Leus, and A. Pandharipande, "Direction estimation using compressive sampling array processing," in *Statistical Signal Processing, 2009. SSP'09. IEEE/SP 15th Workshop on*, pp. 626–629, IEEE, 2009.

[55] A. C. Gurbuz, V. Cevher, and J. H. McClellan, "Bearing estimation via spatial sparsity using compressive sensing," *Aerospace and Electronic Systems, IEEE Transactions on*, vol. 48, no. 2, pp. 1358–1369, 2012.

[56] H. Yu, X. Qiu, X. Zhang, C. Wang, and G. Yang, "Two-dimensional direction of arrival (doa) estimation for rectangular array via compressive sensing trilinear model," *International Journal of Antennas and Propagation*, vol. 2015, 2015.

[57] H. Poor, *An Introduction to Signal Detection and Estimation.* New York: Springer-Verlag, 1994.

[58] T. Kanungo, D. M. Mount, N. S. Netanyahu, C. D. Piatko, R. Silverman, and A. Y. Wu, "An efficient k-means clustering algorithm: analysis and implementation," *IEEE Transactions on Pattern Analysis and Machine Intelligence*, vol. 24, no. 7, pp. 881–892, 2002.

[59] M. K. Steven, "Fundamentals of statistical signal processing," *PTR Prentice-Hall, Englewood Cliffs, NJ*, 1993.

[60] F. Zhang, *The Schur complement and its applications*, vol. 4. Springer Science & Business Media, 2006.

Appendix A

Derivation of the CRLB for a Single Source with Known Complex Amplitude

In this part, the CRLB for $\boldsymbol{\theta}$ is derived when the complex amplitude s is known. To begin with, the mean vector and covariance matrix of $\boldsymbol{y}$ can be derived as follows. If $\boldsymbol{n} \sim \mathcal{N}(\mathbf{0}, \sigma_n^2 \boldsymbol{I}_{MN_T})$, where $\boldsymbol{I}_{MN_T}$ is an $MN_T \times MN_T$ identity matrix, then $\boldsymbol{y} \sim \mathcal{N}(\boldsymbol{\mu}_{\boldsymbol{y}}(\boldsymbol{\theta}), \boldsymbol{\Sigma}_{\boldsymbol{y}}\boldsymbol{\theta})$, where

$$\begin{aligned}
\boldsymbol{\mu}_{\boldsymbol{y}}(\boldsymbol{\theta}) &= \mathrm{E}_{\boldsymbol{n}}\{\boldsymbol{y}\} \\
&= \mathrm{E}_{\boldsymbol{n}}\{\boldsymbol{\mathcal{W}}(\boldsymbol{W})\,\boldsymbol{\Psi}(\boldsymbol{\theta}, \boldsymbol{P}, \boldsymbol{t})\,s + \boldsymbol{n}\} \\
&= \mathrm{E}_{\boldsymbol{n}}\{\boldsymbol{\mathcal{W}}(\boldsymbol{W})\,\boldsymbol{\Psi}(\boldsymbol{\theta}, \boldsymbol{P}, \boldsymbol{t})\,s\} + \mathrm{E}_{\boldsymbol{n}}\{\boldsymbol{n}\} \\
&= \boldsymbol{\mathcal{W}}(\boldsymbol{W})\,\boldsymbol{\Psi}(\boldsymbol{\theta}, \boldsymbol{P}, \boldsymbol{t})\,s \\
&= (\boldsymbol{I}_{N_T} \otimes \boldsymbol{W})\left(e^{j\omega \boldsymbol{t}} \otimes e^{j\omega \boldsymbol{\tau}(\boldsymbol{\theta})}\right) s \\
&= s\left(e^{j\omega \boldsymbol{t}}\right) \otimes \left(\boldsymbol{W} e^{j\omega \boldsymbol{\tau}(\boldsymbol{\theta})}\right)
\end{aligned} \tag{A.1}$$

and

$$\begin{aligned}
\boldsymbol{\Sigma_y} &= \mathrm{E}_{\boldsymbol{n}}\left\{\left(\boldsymbol{y}-\boldsymbol{\mu_y}\right)\left(\boldsymbol{y}-\boldsymbol{\mu_y}\right)^H\right\} \\
&= \mathrm{E}_{\boldsymbol{n}}\left\{\left(\boldsymbol{\mu_y}+\boldsymbol{\mathcal{W}}\left(\boldsymbol{W}\right)\boldsymbol{n}-\boldsymbol{\mu_y}\right)\left(\boldsymbol{\mu_y}+\boldsymbol{\mathcal{W}}\left(\boldsymbol{W}\right)\boldsymbol{n}-\boldsymbol{\mu_y}\right)^H\right\} \\
&= \mathrm{E}_{\boldsymbol{n}}\left\{\boldsymbol{\mathcal{W}}\left(\boldsymbol{W}\right)\boldsymbol{n}\boldsymbol{n}^H\boldsymbol{\mathcal{W}}^H\left(\boldsymbol{W}\right)\right\} \\
&= \boldsymbol{\mathcal{W}}\left(\boldsymbol{W}\right)\mathrm{E}_{\boldsymbol{n}}\left\{\boldsymbol{n}\boldsymbol{n}^H\right\}\boldsymbol{\mathcal{W}}^H\left(\boldsymbol{W}\right) \\
&= \boldsymbol{\mathcal{W}}\left(\boldsymbol{W}\right)\sigma_n^2\boldsymbol{I}_{MN_T}\boldsymbol{\mathcal{W}}^H\left(\boldsymbol{W}\right) \\
&= \sigma_n^2\left(\boldsymbol{I}_{N_T}\otimes\boldsymbol{W}\right)\left(\boldsymbol{I}_{N_T}^T\otimes\boldsymbol{W}^H\right) \\
&= \sigma_n^2\left(\boldsymbol{I}_{N_T}\boldsymbol{I}_{N_T}\right)\otimes\left(\boldsymbol{W}\boldsymbol{W}^H\right) \\
&= \sigma_n^2\boldsymbol{I}_{MN_T}
\end{aligned} \tag{A.2}$$

under the assumption of $\boldsymbol{W}\boldsymbol{W}^H = \boldsymbol{I}_N$. Then, for DoA $\boldsymbol{\theta}$ and measurement matrix $\boldsymbol{W}$, the Fisher Information Matrix (FIM) $\boldsymbol{J}$ can be written as [59]

$$\boldsymbol{J}\left(\boldsymbol{W},\boldsymbol{\theta}\right) = \begin{bmatrix} J_\gamma\left(\boldsymbol{W},\boldsymbol{\theta}\right) & J_{\gamma\phi}\left(\boldsymbol{W},\boldsymbol{\theta}\right) \\ J_{\gamma\phi}\left(\boldsymbol{W},\boldsymbol{\theta}\right) & J_\phi\left(\boldsymbol{W},\boldsymbol{\theta}\right) \end{bmatrix}, \tag{A.3}$$

where

$$J_\gamma\left(\boldsymbol{W},\boldsymbol{\theta}\right) = \frac{\partial\boldsymbol{\mu_y}\left(\boldsymbol{\theta}\right)^H}{\partial\gamma}\boldsymbol{\Sigma_y}^{-1}\frac{\partial\boldsymbol{\mu_y}\left(\boldsymbol{\theta}\right)}{\partial\gamma} + \frac{1}{2}\mathrm{Tr}\left\{\boldsymbol{\Sigma_y}^{-1}\frac{\partial\boldsymbol{\Sigma_y}}{\partial\gamma}\boldsymbol{\Sigma_y}^{-1}\frac{\partial\boldsymbol{\Sigma_y}}{\partial\gamma}\right\}, \tag{A.4}$$

$$J_\phi\left(\boldsymbol{W},\boldsymbol{\theta}\right) = \frac{\partial\boldsymbol{\mu_y}\left(\boldsymbol{\theta}\right)^H}{\partial\phi}\boldsymbol{\Sigma_y}^{-1}\frac{\partial\boldsymbol{\mu_y}\left(\boldsymbol{\theta}\right)}{\partial\phi} + \frac{1}{2}\mathrm{Tr}\left\{\boldsymbol{\Sigma_y}^{-1}\frac{\partial\boldsymbol{\Sigma_y}}{\partial\phi}\boldsymbol{\Sigma_y}^{-1}\frac{\partial\boldsymbol{\Sigma_y}}{\partial\phi}\right\}, \tag{A.5}$$

$$J_{\gamma\phi}\left(\boldsymbol{W},\boldsymbol{\theta}\right) = \frac{\partial\boldsymbol{\mu_y}\left(\boldsymbol{\theta}\right)^H}{\partial\gamma}\boldsymbol{\Sigma_y}^{-1}\frac{\partial\boldsymbol{\mu_y}\left(\boldsymbol{\theta}\right)}{\partial\phi} + \frac{1}{2}\mathrm{Tr}\left\{\boldsymbol{\Sigma_y}^{-1}\frac{\partial\boldsymbol{\Sigma_y}}{\partial\gamma}\boldsymbol{\Sigma_y}^{-1}\frac{\partial\boldsymbol{\Sigma_y}}{\partial\phi}\right\}. \tag{A.6}$$

Using $\frac{\partial\boldsymbol{\Sigma_y}}{\partial\gamma} = \boldsymbol{0}$ and $\boldsymbol{\Sigma_y}^{-1} = \frac{1}{\sigma_n^2}\boldsymbol{I}_{MN_T}$ $J_\gamma\left(\boldsymbol{W},\boldsymbol{\theta}\right)$ can be further expanded as

follows

$$\begin{aligned} J_{\gamma}\left(\boldsymbol{W},\boldsymbol{\theta}\right) &= \frac{1}{\sigma_n^2}\frac{\partial \boldsymbol{\mu_y}\left(\boldsymbol{\theta}\right)^H}{\partial\gamma}\boldsymbol{I}_{MN_T}\frac{\partial \boldsymbol{\mu_y}\left(\boldsymbol{\theta}\right)}{\partial\gamma} \\ &= \frac{|s|^2}{\sigma_n^2}\left(\left(e^{j\omega \boldsymbol{t}}\right)^H \otimes \left(\left(\frac{\partial e^{j\omega\boldsymbol{\tau}(\boldsymbol{\theta})}}{\partial\gamma}\right)^H \boldsymbol{W}^H\right)\right) \\ &\quad \cdot \left(\left(e^{j\omega \boldsymbol{t}}\right) \otimes \left(\boldsymbol{W}\frac{\partial e^{j\omega\boldsymbol{\tau}(\boldsymbol{\theta})}}{\partial\gamma}\right)\right) \\ &= \frac{N_T|s|^2}{\sigma_n^2}\left(\frac{\partial e^{j\omega\boldsymbol{\tau}(\boldsymbol{\theta})}}{\partial\gamma}\right)^H \boldsymbol{W}^H\boldsymbol{W}\frac{\partial e^{j\omega\boldsymbol{\tau}(\boldsymbol{\theta})}}{\partial\gamma} \\ &= \frac{1}{c_0}\left(\boldsymbol{d}_{\gamma}\left(\boldsymbol{\theta}\right)\right)^H \boldsymbol{W}^H\boldsymbol{W}\boldsymbol{d}_{\gamma}\left(\boldsymbol{\theta}\right) \end{aligned} \tag{A.7}$$

where

$$c_0 = \frac{\sigma_n^2}{N_T|s|^2} \tag{A.8}$$

$$\boldsymbol{d}_{\gamma}\left(\boldsymbol{\theta}\right) = \frac{\partial e^{j\omega\boldsymbol{\tau}(\boldsymbol{\theta})}}{\partial\gamma} = \frac{\omega}{c}\left(\boldsymbol{P}_n^T\frac{\partial\boldsymbol{\zeta}\left(\boldsymbol{\theta}\right)}{\partial\gamma}\right) \otimes e^{j\omega\boldsymbol{\zeta}(\boldsymbol{\theta})}. \tag{A.9}$$

Using a similar derivation process, it can be shown that

$$J_{\phi}\left(\boldsymbol{W},\boldsymbol{\theta}\right) = \frac{1}{c_0}\left(\boldsymbol{d}_{\phi}\left(\boldsymbol{\theta}\right)\right)^H \boldsymbol{W}^H\boldsymbol{W}\boldsymbol{d}_{\phi}\left(\boldsymbol{\theta}\right), \tag{A.10}$$

$$J_{\gamma\phi}\left(\boldsymbol{W},\boldsymbol{\theta}\right) = \frac{1}{c_0}\left(\boldsymbol{d}_{\gamma}\left(\boldsymbol{\theta}\right)\right)^H \boldsymbol{W}^H\boldsymbol{W}\boldsymbol{d}_{\phi}\left(\boldsymbol{\theta}\right), \tag{A.11}$$

where

$$\boldsymbol{d}_{\phi}\left(\boldsymbol{\theta}\right) = \frac{\omega}{c}\left(\boldsymbol{P}_n^T\frac{\partial\boldsymbol{\zeta}\left(\boldsymbol{\theta}\right)}{\partial\phi}\right) \otimes e^{j\omega\boldsymbol{\zeta}(\boldsymbol{\theta})}. \tag{A.12}$$

Then, it can be shown that trace of 2×2 inverse Fisher Information is

$$\begin{aligned} \mathrm{Tr}\left\{\boldsymbol{J}^{-1}\left(\boldsymbol{W},\boldsymbol{\theta}\right)\right\} &= \frac{J_{\gamma}\left(\boldsymbol{W},\boldsymbol{\theta}\right) + J_{\phi}\left(\boldsymbol{W},\boldsymbol{\theta}\right)}{\det\left(\boldsymbol{J}\left(\boldsymbol{W},\boldsymbol{\theta}\right)\right)} \\ &= \frac{J_{\gamma}\left(\boldsymbol{W},\boldsymbol{\theta}\right) + J_{\phi}\left(\boldsymbol{W},\boldsymbol{\theta}\right)}{J_{\gamma}\left(\boldsymbol{W},\boldsymbol{\theta}\right)J_{\phi}\left(\boldsymbol{W},\boldsymbol{\theta}\right) - \left(J_{\gamma\phi}\left(\boldsymbol{W},\boldsymbol{\theta}\right)\right)^2}, \end{aligned} \tag{A.13}$$

where $\det\left(.\right)$ denotes determinant operator.

Appendix B

Derivation of the CRLB for a Single Source with Unknown Complex Amplitude

When the complex amplitude s in (2.1) is unknown, the Fisher Information matrix becomes a 3×3 matrix where 3^{rd} row and column are allocated to nuisance parameter s as the following

$$\boldsymbol{J}(\boldsymbol{W}, \boldsymbol{\theta}, s) = \begin{bmatrix} \boldsymbol{J}(\boldsymbol{W}, \boldsymbol{\theta}) & \left(\boldsymbol{J}_{s,\gamma\phi}(\boldsymbol{W}, \boldsymbol{\theta}, s)\right)^H \\ \boldsymbol{J}_{s,\gamma\phi}(\boldsymbol{W}, \boldsymbol{\theta}, s) & J_{ss}(\boldsymbol{W}, \boldsymbol{\theta}) \end{bmatrix}, \tag{B.1}$$

where $\boldsymbol{J}(\boldsymbol{W}, \boldsymbol{\theta})$ is as in (A.3) and

$$\boldsymbol{J}_{s,\gamma\phi}(\boldsymbol{W}, \boldsymbol{\theta}, s) = \frac{s}{c_0} \begin{bmatrix} \left(\boldsymbol{d}_\gamma(\boldsymbol{\theta})\right)^H \boldsymbol{W}^H \boldsymbol{W} e^{j\omega\boldsymbol{\zeta}(\boldsymbol{\theta})} \\ \left(\boldsymbol{d}_\phi(\boldsymbol{\theta})\right)^H \boldsymbol{W}^H \boldsymbol{W} e^{j\omega\boldsymbol{\zeta}(\boldsymbol{\theta})} \end{bmatrix}, \tag{B.2}$$

$$J_{ss}(\boldsymbol{W}, \boldsymbol{\theta}) = \frac{1}{c_0} \left(e^{j\omega\boldsymbol{\zeta}(\boldsymbol{\theta})}\right)^H \boldsymbol{W}^H \boldsymbol{W} e^{j\omega\boldsymbol{\zeta}(\boldsymbol{\theta})}. \tag{B.3}$$

Suppose that the inverse FIM consists of submatrices in the following form:

$$\boldsymbol{J}^{-1}(\boldsymbol{W}, \boldsymbol{\theta}, s) = \begin{bmatrix} \boldsymbol{J}_{\gamma\phi}^{-1}(\boldsymbol{W}, \boldsymbol{\theta}, s) & \left(\boldsymbol{J}_{s,\gamma\phi}^{-1}(\boldsymbol{W}, \boldsymbol{\theta}, s)\right)^H \\ \boldsymbol{J}_{s,\gamma\phi}^{-1}(\boldsymbol{W}, \boldsymbol{\theta}, s) & \boldsymbol{J}_s^{-1}(\boldsymbol{W}, \boldsymbol{\theta}, s) \end{bmatrix}, \tag{B.4}$$

where $\boldsymbol{J}_{\gamma\phi}^{-1}(\boldsymbol{W},\boldsymbol{\theta},s)$ is the 2×2 matrix corresponding to the CRLB of γ and ϕ, $\boldsymbol{J}_{s,\gamma\phi}^{-1}(\boldsymbol{W},\boldsymbol{\theta},s)$ is 2×1 is the matrix representing correlation terms and $\boldsymbol{J}_{s}^{-1}(\boldsymbol{W},\boldsymbol{\theta},s)$ is the CRLB of nuisance parameter s.

Using simple block inversion formula [60], it can be shown that the CRLB corresponding to the parameter of interest $\boldsymbol{\theta}$ is

$$\begin{aligned}\boldsymbol{J}_{\boldsymbol{\theta}}^{-1}(\boldsymbol{W},\boldsymbol{\theta},s) &= \left(\boldsymbol{J}(\boldsymbol{W},\boldsymbol{\theta}) - \boldsymbol{J}_{s,\gamma\phi}(\boldsymbol{W},\boldsymbol{\theta},s)\frac{1}{J_{ss}(\boldsymbol{W},\boldsymbol{\theta})}\left(\boldsymbol{J}_{s,\gamma\phi}(\boldsymbol{W},\boldsymbol{\theta},s)\right)^{H}\right)^{-1} \\ &= \begin{bmatrix} J_{\gamma}(\boldsymbol{W},\boldsymbol{\theta},s) & J_{\gamma\phi}(\boldsymbol{W},\boldsymbol{\theta},s) \\ J_{\gamma\phi}(\boldsymbol{W},\boldsymbol{\theta},s) & J_{\phi}(\boldsymbol{W},\boldsymbol{\theta},s)\end{bmatrix}^{-1}, \end{aligned} \tag{B.5}$$

where

$$J_{\gamma}(\boldsymbol{W},\boldsymbol{\theta},s) = J_{\gamma}(\boldsymbol{W},\boldsymbol{\theta}) - \frac{\left|\left(\boldsymbol{d}_{\gamma}(\boldsymbol{\theta})\right)^{H}\boldsymbol{W}^{H}\boldsymbol{W}e^{j\omega\boldsymbol{\zeta}(\boldsymbol{\theta})}\right|^{2}}{\left(e^{j\omega\boldsymbol{\zeta}(\boldsymbol{\theta})}\right)^{H}\boldsymbol{W}^{H}\boldsymbol{W}e^{j\omega\boldsymbol{\zeta}(\boldsymbol{\theta})}} \tag{B.6}$$

$$J_{\gamma\phi}(\boldsymbol{W},\boldsymbol{\theta},s) = J_{\gamma\phi}(\boldsymbol{W},\boldsymbol{\theta}) - \frac{\left(\boldsymbol{d}_{\gamma}(\boldsymbol{\theta})\right)^{H}\boldsymbol{W}^{H}\boldsymbol{W}e^{j\omega\boldsymbol{\zeta}(\boldsymbol{\theta})}\left(e^{j\omega\boldsymbol{\zeta}(\boldsymbol{\theta})}\right)^{H}\boldsymbol{W}^{H}\boldsymbol{W}\boldsymbol{d}_{\phi}(\boldsymbol{\theta})}{\left(e^{j\omega\boldsymbol{\zeta}(\boldsymbol{\theta})}\right)^{H}\boldsymbol{W}^{H}\boldsymbol{W}e^{j\omega\boldsymbol{\zeta}(\boldsymbol{\theta})}} \tag{B.7}$$

$$J_{\phi}(\boldsymbol{W},\boldsymbol{\theta},s) = J_{\phi}(\boldsymbol{W},\boldsymbol{\theta}) - \frac{\left|\left(\boldsymbol{d}_{\phi}(\boldsymbol{\theta})\right)^{H}\boldsymbol{W}^{H}\boldsymbol{W}e^{j\omega\boldsymbol{\zeta}(\boldsymbol{\theta})}\right|^{2}}{\left(e^{j\omega\boldsymbol{\zeta}(\boldsymbol{\theta})}\right)^{H}\boldsymbol{W}^{H}\boldsymbol{W}e^{j\omega\boldsymbol{\zeta}(\boldsymbol{\theta})}}, \tag{B.8}$$

as $J_{\gamma}(\boldsymbol{W},\boldsymbol{\theta})$, $J_{\phi}(\boldsymbol{W},\boldsymbol{\theta})$ and $J_{\gamma\phi}(\boldsymbol{W},\boldsymbol{\theta})$ are defined in (A.7),(A.10) and (A.11), respectively.

Appendix C

The Derivative of Steering Vectors with respect to Elevation and Azimuth

The cross-correlation terms in the Fisher Information matrix is claimed to be zero when the proposed measurement matrices are used in Theorem 1. Proposition 2 proves such a claim.

Proposition 2. *For symmetric array alignments, the derivative of steering vector with respect to elevation and azimuth, as defined in (A.9) and (A.12), are orthogonal, i.e.,* $\boldsymbol{d}_{\gamma}(\boldsymbol{\theta}) \perp \boldsymbol{d}_{\phi}(\boldsymbol{\theta}) = 0$.

Proof.

$$\begin{aligned}
\boldsymbol{d}_{\gamma}(\boldsymbol{\theta}) \perp \boldsymbol{d}_{\phi}(\boldsymbol{\theta}) &= \boldsymbol{d}_{\gamma}(\boldsymbol{\theta})^{H} \boldsymbol{d}_{\phi}(\boldsymbol{\theta}) \\
&= \left(\frac{\partial e^{j\omega\boldsymbol{\tau}(\boldsymbol{\theta})}}{\partial\gamma}\right)^{H} \frac{\partial e^{j\omega\boldsymbol{\tau}(\boldsymbol{\theta})}}{\partial\gamma} \\
&= \left(e^{j\omega\boldsymbol{\tau}(\boldsymbol{\theta})}\right)^{H} \operatorname{diag}\left(\boldsymbol{P}\frac{\partial\boldsymbol{\zeta}(\boldsymbol{\theta})}{\partial\gamma}\right) \operatorname{diag}\left(\boldsymbol{P}\frac{\partial\boldsymbol{\zeta}(\boldsymbol{\theta})}{\partial\phi}\right) e^{j\omega\boldsymbol{\tau}(\boldsymbol{\theta})} \\
&= \left(e^{j\omega\boldsymbol{\tau}(\boldsymbol{\theta})}\right)^{H} \boldsymbol{D} e^{j\omega\boldsymbol{\tau}(\boldsymbol{\theta})} \\
&= N \operatorname{Tr}\{\boldsymbol{D}\}, \qquad \text{(C.1)} \\
&= 0, \qquad \text{(C.2)}
\end{aligned}$$

where $\operatorname{Tr}\{\boldsymbol{D}\} = 0$ for a symmetric array. □

Therefore, the proposed measurement matrices provide zero cross-correlation terms in the Fisher Information matrices.